University of Bergen
Department of Physics and Technology
Victoria University
Department of Engineering and Science

Master of Science in Measurement Science and Instrumentation

Detection of CO_2 in N_2 and H_2O using photoacoustics

Vårin Renate Andvik Holm

2012-2013

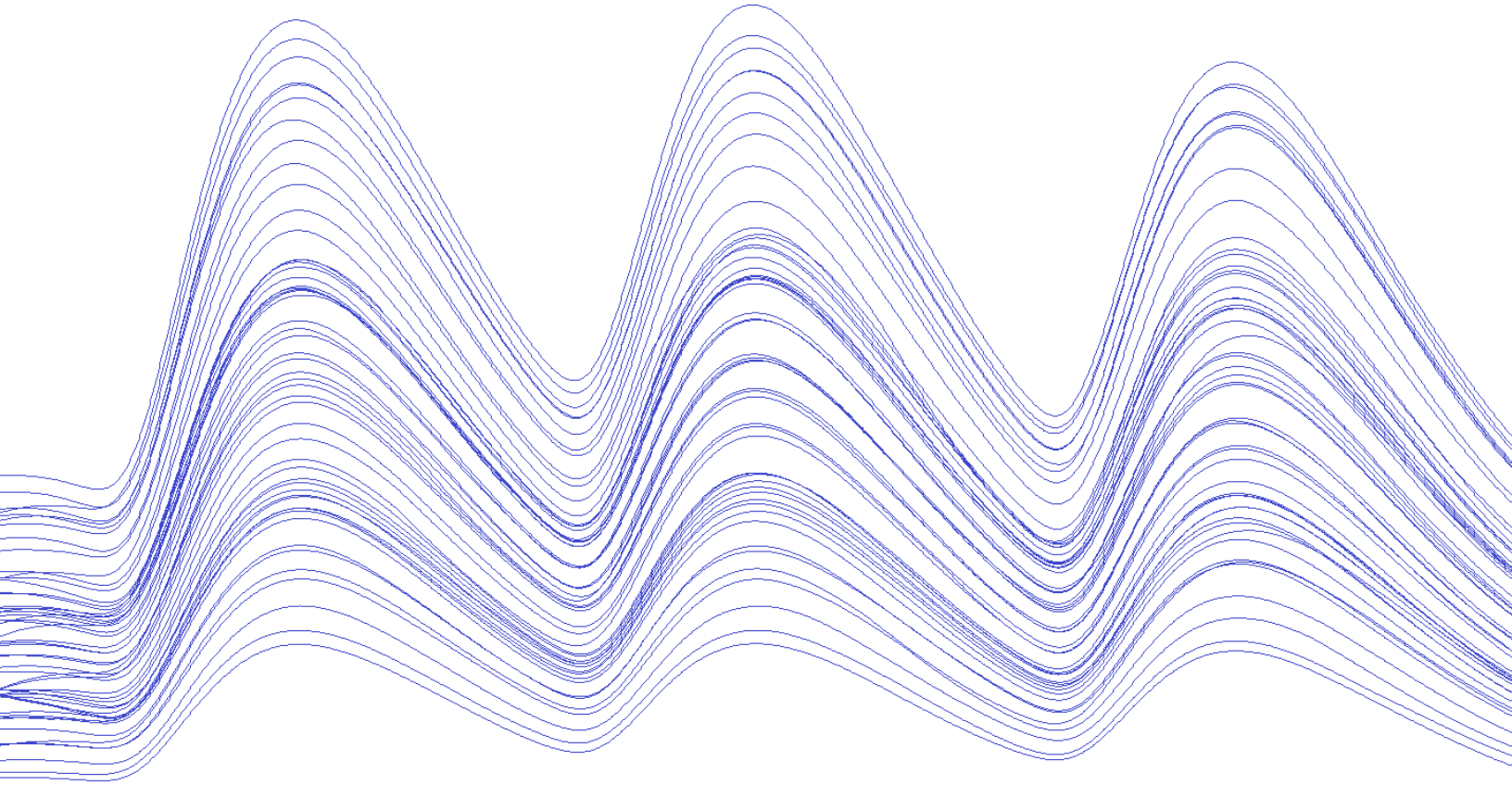

"Highly diathermanous bodies, I reasoned, would produce faint sounds, while highly athermanous bodies would produce loud sounds; the strength of the sound being, in a sense, a measure of the absorption"

-Professor John Tyndall, 1881.

Abstract

Photoacoustic spectroscopy is a technique where absorbed modulated light is released as heat, causing thermal expansion which can be detected using an acoustic transducer. It can be used to determine the absorption spectra or the concentration of a material. In this project, photoacoustic spectroscopy is performed on CO_2 in N_2 gas and on CO_2 dissolved in water in the $2003-2006$ nm range. Studies on CO_2 concentrations can be used in environmental research and fish industries, to mention some applications.

Linearity in the signal is demonstrated for concentrations over several orders of magnitude for the gas mixture. The effect of water vapour in the sample is investigated, and the optimal modulation frequency and other relevant factors are determined.

For the water sample, different measurement cell configurations are investigated before achieving a photoacoustic signal. With the final configuration used, high concentrations of CO_2 in water can be detected indirectly through a small layer of inert gas above the water. Smaller concentrations can not be detected due to a high noise level.

Together with instruments for generating and modulating laser light and for detecting the acoustic signal, a gas sample measurement cell and a water sample measurement cell form the experimental setup. LabVIEW from National Instruments is used to develop a software for instrument control, data acquisition and data analysis.

Acknowledgements

Thanks to my SUPERvisor Bjørn Tore Hjertaker for you subtle hint about which project was the BEST one. Your always open door policy and willingness to help with anything at all made the independent work seem fun rather than scary. Thanks for all the cheerful chats in your office and your encouragement along the way. The lesson I appreciate the most is independent learning, and to trust my own reasoning. I'm still impressed you left me alone with that laser to hook it up, trusting I wouldn't break it. Also thanks to Erik Magnus Bruvik for being an eager contributor, and for helping me to see new solutions when I get stuck. Your input has been most helpful and appreciated.

I am very thankful for the resources UIB has provided me with. Among the staff at UIB, I would especially like to thank Magne Vestrheim, Lars Egil Helseth and Rachid Maad for answering my questions about acoustics, optics and electronics, and for helping me choose the right equipment to use. Roald Langøen and the guys down at the workshop have been real champs, making all sorts of wonderful things for my project. I'd also like to give a shout out to my fellow students Alexandre Vial who taught me LabVIEW and made the lab-course go fast and easy, and Tonje Opkvitne who's always up for a chat in the optics-lab.

The financial support from Michelsen Centre for Industrial Measurement Science an Technology has been very much appreciated. The laser with all it's equipment, the waveform generator, the hydrophone, microphone and amplifiers, the optics and the computer have become fun "toys", and I've learned so much using them.

I also learned much during my stay at Victoria University. I would like to thank my supervisor Thinh Nguyen for receiving me and buying me that cup of coffee the first day. Also, thanks for sticking me in the same lab as Fotios

Sidiroglou. You both taught me a lot, and made my first experience working in a lab a very pleasant one.
To my family, I would like to say thanks fo shaping me into the person I am, for teaching me good values, and for cheering me on. Thanks to my Dad for never answering a question with "I don't know", to my Mum for always ending a physics discussion at the dinner table with "Well, however it works, it must be well created". To my brothers Lidvar, Christer, Eldar and Erlend for being among the smartest people i know, each in their own way. To my sisters in law Inese and Miyuki, and my nieces and nephew Matias, Mei and Aija, for contributing to the fun chaos that is any family gathering. To my hubby Thorbjørn, thank you for hearing what I mean and not what I say.
Finally, I would like to thank my diving instructor Paul Joachim Thorsen and my tricking gym Fysak for attaching my head back on my neck every time it exploded after spending too much time in the lab. The number of times you saved it is un-countable.

Contents

Abstract **iii**

Acknowledgements **v**

Contents **vii**

List of Figures **x**

List of Tables **xiv**

1 Introduction **1**

1.1 What is photoacoustic spectroscopy? 1

1.2 History 3

1.2.1 Discovery to invention 3

1.2.2 From the 1980's to present on PAS performed on gas . 4

1.2.3 From the 1980's to present on PAS performed on solids 5

1.2.4 From the 1980's to present on PAS performed on liquids 5

1.3 Applications and motivation 6

1.3.1 General 6

1.3.2 When other techniques do not work 7

1.3.3 Adding of spectra 7

1.3.4 Minimal preparation 8
1.3.5 Depth profiling 8
1.3.6 Confirmation and supplementation to other methods . 8
1.3.7 PA does not destroy the sample 9
1.3.8 Higher sensitivities 9
1.4 This Project 10

2 The photoacoustic principle 11

2.1 The physics of photoacoustics 11
2.1.1 General 11
2.2 Optical setup 17
2.2.1 Light source 17
2.2.2 Optical fibre and polarisation 19
2.2.3 Collimation. 21
2.2.4 Optomechanics 21
2.3 Acoustic setup 23
2.3.1 Sound detection 23
2.4 Other setup 26
2.4.1 Lock-In Amplifier 26
2.4.2 Measurement cell 28
2.4.3 Gas flow controlling equipment 31
2.4.4 Data acquisition 32

3 Measuring CO_2 in air 35

3.1 Materials and Methods 36
3.2 Experiments 39

3.2.1 Basic initial experiment 39

3.2.2 Amplitude vs phase modulation, excitation frequency and other parameters 44

3.2.3 LabVIEW 48

3.2.4 Characterising the laser diode 53

3.2.5 The effect of water 55

3.2.6 Linearity of PA signal with regard to concentration . . 58

3.2.7 Measurement uncertainty 62

4 CO_2 in water 67

4.1 Models and methods 67

4.2 Experiments 70

4.2.1 Investigating frequencies and wavelengths in search of a signal 70

4.2.2 Trouble shooting 71

4.2.3 Achieving PA signal 76

5 Conclusion 79

5.1 Further work 81

5.1.1 Ocean water 81

5.1.2 Experimenting with the configuration 81

5.1.3 Prototype 82

References 83

Appendix A 87

List of Figures

1.1 Number of articles published using the key phrase "photoacoustic spectroscopy" from the early 1970s to 2005 (Ball, 2006) 4

1.2 PAS used to detect melanoma. (Freeman, 2012) 6

2.1 The PA principle. 12

2.2 Illustration of the propagation of the acoustic waves generated by PA from for barely absorbing and highly absorbing sample materials (Schmid et al., 2009). 14

2.3 Illustration of the PA effect (Patel and Tam, 1981), (Zhao and Zuomin, 2002). 16

2.4 Illustration of total internal reflection (Nguyen, 2010). 20

2.5 Illustration of Brewster angle (Nguyen, 2010). 20

2.6 Illustration of the collimation principle. 22

2.7 Illustration of a condenser microphone. 24

2.8 Directivity pattern of *Brüel&Kjœr* type 8103 hydrophone. . . 25

2.9 A very simple block diagram of the principle of the lock-in amplifier 27

2.10 The PA measurement cell for gas detection 29

2.11 The PA measurement cell for water detection 31

2.12 Illustration for calculating distance from source for a plane wave approximation. 31

2.13 Flow controllers mixing the gas 33

3.1 Initial PA set-up. 37

3.2 Final PA setup at UIB. 38

3.3 Absorption coefficients from HITRAN. The difference between atmospheric air and pure CO_2 is due to H_2O which may vary depending on relative humidity. 41

3.4 First PA sweep, performed at Victoria University. The values of the PA signal are relative. 42

3.5 PA signal with varying CO_2. The syringe method is not accurate, but the general idea of increasing signal with increasing CO_2 concentration is conserved. The signal seem disturbed at initial data-points for the increasing CO_2 plot. 43

3.6 Three different ways to modulate the laser. Produced with $f = 1310\ Hz$, $sens = 1e{-}3$, $timeconst = 3\ s$. The current was $I = 10 - 100\ mA$ for amplitude modulation and $I = 95 - 105\ mA$ for phase modulation. The measurement cell was filled with air. 47

3.7 Determining the resonance frequency. 47

3.8 Sensitivity of LIA varied. 48

3.9 Initialising the waveform generator. 50

3.10 Initialising the LIA. 50

3.11 Initialising the LD/TC controller 51

3.12 Main section of VI where temperature sweep is performed and LIA data is read. 51

3.13 Wavelength variations with temperature and current. 52

3.14 Laser diode characteristics. Threshold current of the nanoplus laser diode is approximately 12 mA. 54

3.15 Water vaporising affecting the PA signal. 57

3.16 Adding the CO_2 signal with the H_2O signal. 57

3.17 PA signal mean and standard deviation for concentration measured with a sensitivity of $500e-6\ V$. 61

3.18 Maximum value of 2004.5 nm peak for various concentrations. 61

4.1 Initial experimental set-up for experiments in water. 71

4.2 Frequency scan done with $T = 38^o\ C$ with and without the laser turned on to determine if PA signal is achieved and to investigate noise level. 72

4.3 Absorption coefficient of water, (Wieliczka et al., 1989) 73

4.4 Improved experiment set-up for measurements in water 76

4.5 The PA signal from the water sample decrease with time until settling at a certain value. Figure 4.5a shows this in a 3D plot, while figure 4.5b shows the maximum value of the three peaks from figure 4.5a changing with time. 78

List of Tables

3.1 The concentrations and sensitivities that are used, and the result for the frequency sweep. 60

3.2 The gradient, offset and regression value of the four slopes shown in figure 3.18 63

3.3 Measurement uncertainties of the various components in the PA setup. An interfering input causes a constant deviation from the desired value, whereas a modifying input is a systematic error, where the size of the error depends on some variable. 65

3.4 Measurement uncertainty based on repeatability 65

4.1 The density, speed of sound and acoustic impedance are given for water, stainless steel and air (NDT Resource centre), (Cobbold, 2007). 68

5.1 Listed content of appended CD. 87

Abbreviations

ADC - Analogue to digital converter
AR - Anti reflection
DFB - Distributed feedback
DSP - Digital signal processing
FT-IR PA - Fourier transform infrared photoacoustics
IR - Infrared
LD - Laser diode
LED - Light emitting diode
LIA - Lock-in amplifier
MAX - Measurement and Automation Explorer
NIR - Near infrared
PA - Photoacoustic
PAS - Photoacoustic spectroscopy
PZT - Piezoelectric transducer
QCL - Quantum cascade laser
SNR - Signal-to-noise ratio
TEC - Thermoelectric cooling
UIB - University of Bergen
VU - Victoria University

Chapter 1

Introduction

1.1 What is photoacoustic spectroscopy?

Photoacoustic (PA) spectroscopy is a spectroscopy technique where light absorbed by a material causes a pressure wave to propagate. The original experiment performed by A. G. Bell in 1880 involved the use of sunlight, and the pressure wave was detected by the ear. Since then, the principle of the theory has been more or less the same, but developed to be more sensitive, allowing smaller quantities of the absorbent material to be measured.
In modern PA, the light source is a laser. The wavelength of the laser depend on what is being measured. Different materials absorbs at different wavelengths. If a spectra is to be obtained, the wavelength needs to vary. The sample can be kept inside a measurement cell, or it can be in the open. Having an open ended measurement setup is an advantage because it allows measurements to be done on samples that cannot be removed from its environment. However, a measurement cell can be designed to resonate at the preferred modulation frequency, amplifying the signal. This allows for smaller sensitivity limits than what the open end measurement cell would allow for. The use of multiple microphones to achieve more sensitive measurements using an open cell configuration has been tested and proven useful by Markus Sigrist on many occasions (Michaelian, 2010).
Photoacoustic spectroscopy has proven to hold some advantages over traditional spectroscopy. The sample needs little or no preparation prior to the measurement. It is suitable for opaque materials, and depth profiling can be

done for inhomogeneous or layered solids (Michaelian, 2010).

When the light enters the sample, the material in question will absorb the energy of the light. In order for the process to be photoacoustic, the molecules need to get rid of the absorbed energy through a non-radiative relaxation process. The energy is in this way converted into thermal energy. The part of the sample that the laser ray encounters will expand, resulting in a pressure wave propagating outwards from the laser beam. By having a modulated laser, the pressure wave will occur periodically, and can be detected as an acoustic wave. The intensity of the acoustic wave reflects how much energy has been absorbed by the sample, and the frequency of the acoustic wave will be equal to the modulation frequency of the laser. The acoustic signal can be measured using a sensitive microphone or a piezoelectric transducer, depending on the physical state of the sample. This project includes monitoring of CO_2 in both gas and water, so both a microphone and a hydrophone has been used. The photoacoustic signal is potentially very small. By using a lock-in amplifier, the photoacoustic signal can be detected in noise many times larger than that of the actual signal.

Mainly three things has been improved in PA spectroscopy since it was discovered. First, the use of lasers instead of sunlight allows for higher resolution of the spectra, since the bandwidth of the laser is much narrower. Second, the use of sensitive microphones or piezoelectric transducers allows quantitative results rather than that obtained by the ear. Third, optimised measurement cells can resonate, increasing the sensitivity of the measurement (Patel and Tam, 1981).

PA spectroscopy can be performed in a large range of wavelengths, and the sample can be gas, solid or liquid. These parameters result in a set of different measurement setup. For example, a sensitive microphone can be used for a gas sample, whereas a piezoelectric transducer is better suited for the detection of pressure waves in liquids.

1.2 History

1.2.1 Discovery to invention

Photoacoustics is mentioned in literature as far back as 1881, by W. C. Röntgen, A. G. Bell and J. Tyndall (Rosencwaig, 1973). They were looking for a simplified way to test the relationship between radiant heat and gaseous matter. Tyndall used the original experiment of Bell where sound was produced by exposing a periodic beam of light to a solid body. The idea was that diathermanous (heat transparent) bodies would result in a weak sound, whereas atheromanous (heat absorbing) bodies would result in louder sounds. The volume would thus be a measure of the absorption (Tyndall, 1881).

From 1881 to the 1970's, the technique was occasionally used to determine the absorption as a function of wavelength for gases, but offered little advantage over conventional spectroscopy. In 1938 M. L. Viengerov used photoacoustics for gas analysis, but his results were limited by the sensitivity of the microphone and undesired photoacoustic effects (Rosencwaig, 1980). The photoacoustic progress was therefore slow or absent during this period.

Einstein introduced the theoretical foundation for the laser in 1917, and it was developed late in the 1950's. With the introduction of lasers the sensitivity could be considerably increased. Photoacoustic spectroscopy (PAS) research turned out to grow exponentially during the 1970's and 1980's. Figure 1.1 show the number of publications made on the subject between 1975 and 2005.

Between 1978 and 1980 multiple wavelength PAS was developed, particularly PA Fourier transform infrared spectroscopy (FT-IR spectroscopy). FT-IR spectroscopy allows for a light source with a wide spectral range to be used, making measurements for a wide range of wavelengths simultaneously. A Fourier transform is needed to separate the various signals, hence the name. Important contributors to the PA FT-IR spectroscopy theory are Rockley and his collaborators, Vidrine and his collaborators, and Mead (Michaelian, 2010).

In 1980 Rosencwaig published the first book on the subject called "Photoacoustics and photoacoustic spectroscopy", in which the general theory was explained. Since 1980 there has been roughly between 30 and 60 publications

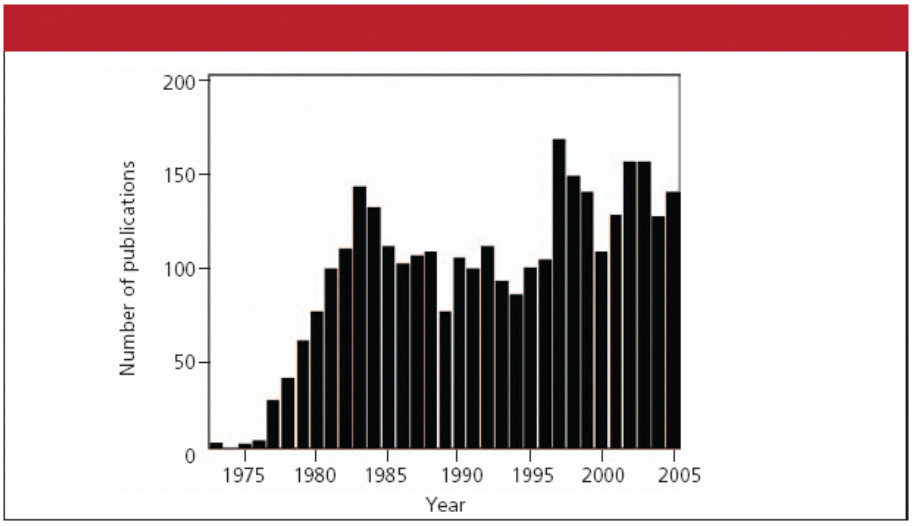

Figure 1.1: Number of articles published using the key phrase "photoacoustic spectroscopy" from the early 1970s to 2005 (Ball, 2006)

each year, developing the opportunities for detection of traces in gas, solids and liquids.

1.2.2 From the 1980's to present on PAS performed on gas

The most prominent researcher on PA of gas is probably Markus W. Sigrist. Many articles have been written or co-written by him using CO lasers, CO_2 lasers and difference-frequency generation, to detect various gases. A summary of different PA development techniques was also published in "Air Monitoring by Spectroscopic Techniques" in 1994.
Despite the vast increase in research on PA since the 1980's, particularly within gas detection, new features in the PA spectra still emerge. Merker et al. in his 1999 paper experienced this while working with high-resolution spectra of $HCOOH$ vapour.
In 2007, Grossel et al. investigated NO bands and H_2O bands. This experiment is an example of how well PA can work even for low laser powers, and a 3 mW laser was used to achieve a detection limit of 20 ppb.

1.2.3 From the 1980's to present on PAS performed on solids

In the period between 1983 and 1991 Low et al. published a series of articles concerning PAS done on carbons. An absorption band at 6.25 μm was observed in the spectra of many different carbons. Low and Morterra observed a dip near 7.41 μm which lead to the 6.26 μm to be thought of as the infrared analogue to the Raman 'G' band, and that Raman and infrared spectra are in fact complimentary.
Work was done on semi-solids by Schendzielorz et al. in 1999 and Hanh et al. in 2000 by studying drug penetration from a semi-solids into dodecanol-collodion membranes, i.e. membranes meant to mimic the skin. The bands caused by the drugs increased with time and diffusion constants was calculated. Figure 1.2 show a PA setup to study melanoma, which is another interesting study of solids from the world of medicine.

1.2.4 From the 1980's to present on PAS performed on liquids

PAS on samples in water is difficult. A problem often occurring when doing PAS on solids containing significant amounts of water, is that the water is evaporated by the heat generated by the absorption of the laser light. Consequently, the PA spectra appears to show bands corresponding to water vapour rather than water moisture in the sample. This is demonstrated by Yang and Irudayaraj in 2000 related to PAS on e.g. butter.
Successful publications on PA experiments related to liquids can be found. In the analysis of chocolate and coca liquors, Belton, Saffa, and Wilson (1988) compared ATR IR spectroscopy with PAS. Both spectra showed good results. Favier et al. investigated contaminants in extra-virgin olive oil. A laser was used in a region where the olive oil does not absorb significantly. However, safflower and sunflower oil does, allowing the amount of these oils in the olive oil to be detected. The detection limit was found to be around 5%, a high number compared to the detection limits achieved for gas traces.

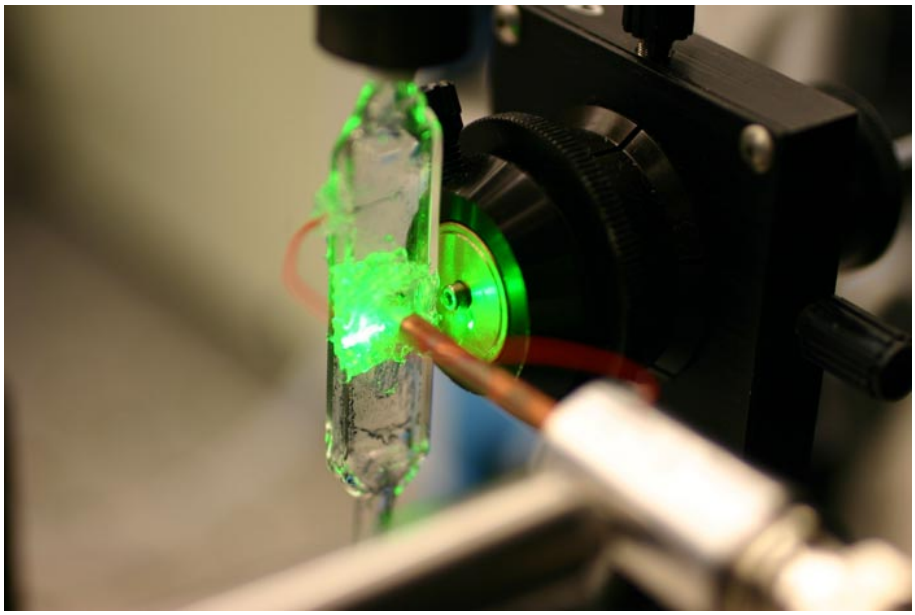

Figure 1.2: PAS used to detect melanoma. (Freeman, 2012)

1.3 Applications and motivation

The following sections is inspired by Kirk H. Michaelian's book "Photoacoustic IR Spectroscopy" (2010). The book is one of very few books written on the subject. The chapter on PAS applications summarises the main contributions by PAS, and provides a good overview of articles in various fields of science. It is the only recent complete summary, containing work up to 2010.

1.3.1 General

The applications and motivation for using PAS are closely linked. Being a fairly new technique compared to other spectroscopy methods, it is not a given that PAS should be preferred. Traditional methods have been tried extensively, and its results verified. The motivation for using PAS lies in the advantages it hold over other techniques.

1.3.2 When other techniques do not work

A definite advantage of the technique lies in the capabilities for the analysis of otherwise problematic or even impossible samples. In spectroscopy, the absorption of a sample is measured as a function of wavelength. Often, the requirement for infrared spectra of solid state catalysts present a challenge. Many heterogeneous catalysts are supported on substrates which strongly absorb or scatter light, like alumina, silica and metal oxides, and the scattering affect of the infrared and Raman spectra.
Luo et al. concluded in his 1994 paper that PAS was superior to infrared transmission and circular dichroism spectroscopy after studying the PA spectra of four different proteins. This was quite a statement considering the fact that circular dichroism spectroscopy is a commonly used technique for studying protein. In some cases, preparation for traditional spectroscopy might change the structure of the sample and give misleading results. For example, ATR spectra were influenced by the removal of hydrating water in a protein sample. In the solid state, differences in the PA and KBr pellets spectra indicated that the preperation might cause protein denaturation (tertiary and secondary structure is lost due to external stress). If done on a protein in a living cell, the cell may die.

1.3.3 Adding of spectra

Kirshnan, in 1981, subtracted the spectra of acetylsalicylic acid from the spectra of a mix of acetylsalicylic acid and phenacetin. The result was a spectra practically identical to phenacetin. This demonstrates that the spectra of drugs can be added, which is a convenient feature (Krishnan, 1981). Repond and Sigrist also demonstrated this feature (Michaelian, 2010).
A technique concerning subtraction of the PA spectra from filters is occasionally used. The PA spectra of a clean sheet of filter paper is subtracted from the spectra of oil or a solid deposited on the filter. This way the spectra of the intended material can be found.

1.3.4 Minimal preparation

Before measuring the IR spectra of carbons, it needs to be finely divided and dissolved in an infrared-transparent diluent. In spectral analysis of coal, extensive grinding and dispersion in alkali halides are required for the classical transmission technique. This is a time consuming approach, and leads to heating and oxidation, among other disadvantages. The elimination of diluent simplifies the experiment. Among the samples that benefit greatly from the small preparation required in PAS are semi-solids like ointments or creams, human hair, grains, clay, minerals, water, bacteria and other organic matter. PAS has also been performed on wool. Since PAS is so insensitive to sample morphology, it is a good technique to use.

1.3.5 Depth profiling

Depth profiling has been proven useful in the study of teeth and nails. Over 270 articles have been written on the subject of PA spectra of polymers, and the reason for this popularity is the possibility of depth profiling of polymer laminates. Depth profiling have been performed on wool by Carter, Fredericks, and Church in 1996, and on potato chips by Sivakesava and Irudayaraj in 2000. The technique was used by Pandey and Vuorinen in 2008 to investigate the degradation of wood caused by UV (laser) light. It has also been used to investigate the layers in coated paper. Bands were identified in a PA spectra obtained by Halttunen et al. in 1999, showing that sodium oleate concentration was higher on the surface of paper coating. This level of detail demonstrate the versatility of depth profiling.

1.3.6 Confirmation and supplementation to other methods

PAS can be combined with other spectroscopy methods to confirm or verify data already found using other techniques. In the 1970's and 1980's, during the so-called demonstration phase of PAS, polymers were often used to demonstrate the validity of PAS. Later, in 1991, the studies of Butler, Li

and Gao showed that for mid-infrared PA spectra of certain samples, the ATR and transmission spectra had more or less the same intensities. In the near-infrared region, PAS was more sensitive.

1.3.7 PA does not destroy the sample

In preparing the sample, some of the information concerning the sample may be lost. Yang and Irudayaraj published a paper in 2001 on ATR and PA spectroscopy preformed on various types of meat. Instead of solving the protein in a solvent, and either emulsifying or extracting and refining fat, information was obtained on the moisture distribution by depth profiling, and a difference could be seen in the spectra for different meats.
In 1988, Kuo et al. investigated transverse and oblique sections of ponderosa pine. The two spectra showed differences due to the fact that cellulose chains were oriented differently. This difference would not occur in a ground sample.
Sometimes the sample may be valuable, or irreplaceable. In 1984 Low, Morterra, and Severdia investigated a piece of paper from 1577. The spectra of the paper was found, and the spectra of a blue spot on the paper which turned out to be a type of mould.

1.3.8 Higher sensitivities

In gas analysis, PAS has a clear advantage due to the very high sensitivity that can be achieved. Many PA trace gas analysis has achieved sensitivities in the range of ppm and even ppb.
Persijn and co-workers used PAS to study the gases released in the prosess of ripening fruit. Bijnen et al. achieved ppb levels in their studies of arthropods. The high sensitivity in PAS for trace gases makes it very relevant in pollution monitoring and toxic gas detection.
One of the most impressive concentration levels detected in PAS was preformed by M. W. Sigrist and co-workers, who has made major contributions to PAS of gases. They achieved a detection limit of 70 *ppt* (parts per trillion) for C_2H_4, This particular experiment was published in 2000. Around the same time, Sigrist preformed experiments of various gases revealing dynamic ranges up to seven orders of magnitude.

1.4 This Project

During the later years we have become more concious concerning environmental effects from CO_2 pollution. Some of the CO_2 resides in the atmosphere, and about 30% of the CO_2 from combustion of fossil fuel is absorbed by the ocean. Storms systems like El Niño stir up the ocean making it emit CO_2 instead of absorbing it. Following, speculations have been made that the earth's CO_2 reservoirs are full (Keeling and Charles, 2004). A lot of research has been done on CO_2 in the atmosphere, but not much has been done relating to the CO_2 levels in the oceans. The CO_2 content in water affects plants, fish and animals living in it. Research has shown that high CO_2 content may cause brain damage and can affect the nervous system in fish (Herbert and Bronwyn, 2012). Two of the best examples for applications of PA in CO_2 monitoring is for environmental research and for fish industries. The high sensitivity and large dynamic range of PA spectroscopy makes it ideal for detecting pollutions in air. PA spectroscopy has proven to be harder to do in liquids, due to the absorption occurring in the liquid. However, choosing the right wavelength for the laser light can minimise this effect. If successful, the technique can be used in pollution monitoring in water for environmental or fish industry purposes, just to mention a few examples.
The goal of this project is to establish if it is possible to develop a relatively cheap, low powered PA instrument to detect CO_2 in both gas and water. High power lasers, which would give strong PA signals, require a lot of power and safety precautions, and are expensive. This should be avoided, so a requirement for the PA instrument in this project is to use a relatively low power laser.

Chapter 2

The photoacoustic principle

Figure 2.1 shows the general principle of a photoacoustic experiment. In this chapter a closer look at different components and processes related to the experimental work in this project will be taken. First, a physical explanation of the PA phenomenon is given, followed by an explanation of the components that utilises it.

2.1 The physics of photoacoustics

2.1.1 General

PAS relies on laser light being absorbed, followed by a non-radiative relaxation process creating pressure waves. The light of the laser carries a certain amount of energy E_0, which can be absorbed to a varying degree depending on the absorption coefficient α of the absorbing material and the path length l of the laser beam.

$$E_{abs} = E_0(1 - e^{-\alpha l}) \tag{2.1}$$

E_{abs} is the absorbed energy. The absorption coefficient is frequency dependent, and different absorption peaks correspond to different materials.
Attenuation in optics can be described by two categories: Scattering and absorption. Absorption mainly happens through two processes. First, electrons can absorb a photon to reach an exited state. This happens for frequencies in the UV and visible range. Secondly, atomic and molecular structure like

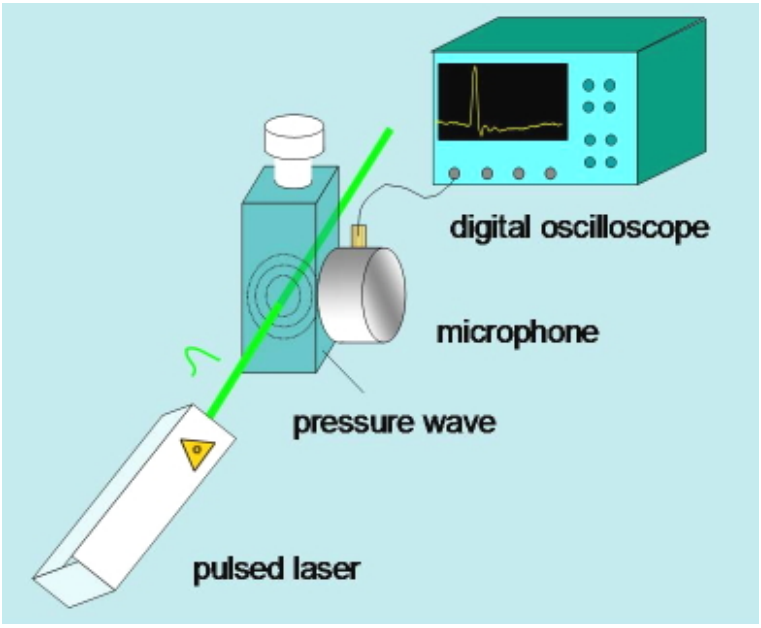

Figure 2.1: The PA principle.

molecular vibrations, chemical bonds and density of molecules can cause absorption in the IR, far IR , radio and microwave range. It is this second type of absorption that distinguishes between materials.

Assuming that radiative relaxation processes can be neglected, all the absorbed energy is converted into heat. The local temperature rise depends on the specific heat capacity C_p, and the thermal expansion is determined by the thermal expansion coefficient β (Schlageter et al., 1997). Assuming no viscous losses, the pressure wave equation can be expressed as

$$\nabla^2 p - \frac{1}{c^2}\frac{\delta^2 p}{\delta t^2} = -\frac{\beta}{C_p}\frac{\delta H}{\delta t} \tag{2.2}$$

where c is the speed of sound, β is the volumetric expansion coefficient and H is a function defined as the heat deposited in the medium per unit volume and time (Zhao and Zuomin, 2002). However, losses do occur, due to viscosity and thermal conduction (Bijnen et al., 1996).

The reason we are distinguishing between gas, liquids and solids, is mainly because of the big variation of the absorption coefficient. If the optical penetration depth is much larger than the length of the cell, $\alpha_a l << 1$, the illuminated volume will have a cylindrical shape, and the acoustic wave will propagate radially. The electro-acoustic transducer should then be placed on the side so that it can pick up the radial sound and not be affected by the

laser light. If the optical penetration depth is much shorter than the length of the cell, $\alpha_a l >> 1$, all the light will be absorbed at the beginning of the cell. The acoustic signal is then approximated to come from a point source, and the signal will propagate spherically. In this case the electro-acoustic transducer must ideally be curved or placed a sufficiently distance from the source in order for the sound waves to be plane when hitting the electro-acoustic transducer. Figure 2.2 illustrates this point (Schmid et al., 2009).
The following is based on the derivation given by Patel and Tam in their 1981 article "Pulsed optoacoustic spectroscopy of condensed mater". The goal is to show how the absorption is related to the measured signal from the electro-acoustic transducer. Imagine a sample illuminated by a laser. The laser is pulsed producing a pulse of duration τ_L at a repetition rate f. The energy absorbed by the sample E_{abs} is related to the laser puls energy E_0 by eq. 2.1, where α is the absorption coefficient and l is the length of the medium. A linear expansion of E_{abs} gives:

$$E_{abs} = E_0 \alpha l \tag{2.3}$$

We require that the energy relaxation is non-radiative, making $E_{abs} = E_{th}$, where E_{th} is the thermal energy. The thermal energy is related to the change in temperature ΔT of the iluminated region. If C_p is the specific heat at constant pressure, V is the volume and ρ is the density of the sample, E_{th} is given by

$$E_{th} = C_p V \Delta T \rho \tag{2.4}$$

Rearranging equation 2.3 and 2.4, an substituting $V = \pi R^2 l$ where R is the radius of the illuminated region, gives:

$$\Delta T = \frac{E_0 \alpha}{\pi R^2 C_p \rho} \tag{2.5}$$

Depending on the shape of the light pulse and the penetration depth, the expression for the pressure amplitude may vary. The laser pulse time length is defined as τ_L. τ_a is the transit time, the time the acoustic pulse travels across the radial direction of acoustic source. For $\tau_L >> \tau_a$, and $\alpha l << 1$, there is an adiabatic, isobaric expansion. Adiabatic expansion means that there is no heat transfer between the system and its environment, isobaric expansion means the pressure is held constant through the expansion process.

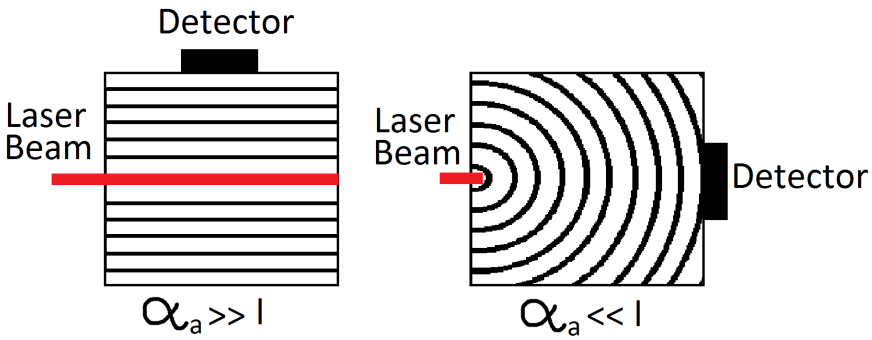

Figure 2.2: Illustration of the propagation of the acoustic waves generated by PA from for barely absorbing and highly absorbing sample materials (Schmid et al., 2009).

The illuminated column will expand, increasing the radius by

$$\Delta R = \frac{1}{2} R\beta\Delta T \tag{2.6}$$

The expansion of the illuminated column creates a pressure wave p propagating radially outwards from the column, which can be expressed as:

$$p = 2\pi f_a c\rho K'\Delta R \tag{2.7}$$

where K' is a constant dependent on the geometry of the laser beam, and f_a is the frequency of the pulsed laser. The expressions given in equation 2.5 and 2.6 can be assembled into 2.7. The geometry of the laser beam is fixed and the speed of sound is constant, so R and c is included in the constant K'. An electro-acoustic transducer converts the pressure wave into an electric potential by a conversion factor G specific to the transducer in use.

$$V_{PA} = Gp = GK'\frac{\beta f_a}{C_p} E_0\alpha \tag{2.8}$$

for a given frequency f_a. Four characteristic pulse shapes can be generated from the photoacoustic setup:

- $\alpha l << 1$ and $\tau_L >> \tau_a$, i.e. the optical penetration depth is much longer than the length of the cell, and the laser pulse time length is much longer than the transit time.
- $\alpha l << 1$ and $\tau_L << \tau_a$, i.e. the optical penetration depth is much longer than the length of the cell, and the laser pulse time length is much shorter than the transit time.
- $\alpha l >> 1$ and $\tau_L >> \tau_a$, i.e. the optical penetration depth is much shorter than the length of the cell, and the laser pulse time length is much longer than the transit time.
- $\alpha l >> 1$ and $\tau_L << \tau_a$, i.e. the optical penetration depth is much shorter than the length of the cell, and the laser pulse time length is much shorter than the transit time.

The equation for the pressure amplitude is proportional to the absorption coefficient α for the different pulse shapes, but the constant K' will be different for the different shapes(Zhao and Zuomin, 2002). Figure 2.3 illustrates a cylindrical propagation of the acoustic wave in matter with $\alpha l << 1$ together with the two shapes mentioned for highly absorbing samples, i.e. the two last bullet points.
The voltage measured with the electro-acoustic transducer will be directly proportional to the input pulse energy E_0 and the absorption coefficient α. The energy transfer of the acoustic wave to the detector depends on the acoustic impedance Z, which in turn depends on the density ρ and speed of sound c.

$$Z = \rho c \tag{2.9}$$

The pressure transmitted to the acoustic detector/transducer p_T depends on the impedance of the medium, Z_{med}, and the transducer, Z_{trans}, and the pressure that has reached the interface, p_0 (Schmid et al., 2009).

$$p_T = p_0 \frac{2Z_{trans}}{Z_{trans} + Z_{med}} \tag{2.10}$$

PAS can be conducted in many ways. One way of classifying PA techniques is as continuous-wave or pulsed mode. In continuous-wave, the duty cycle of the modulated beam is 50%. This technique introduces a heating effect on

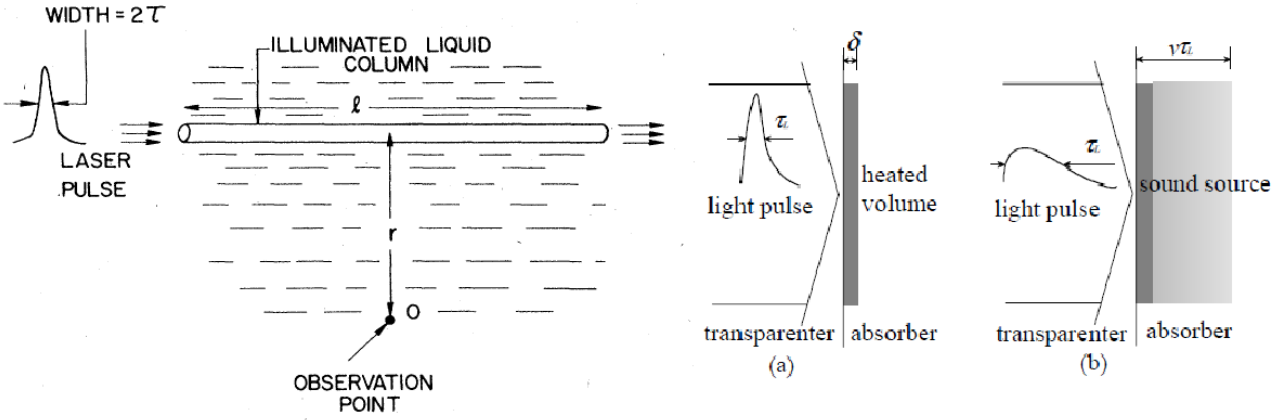

Figure 2.3: Illustration of the PA effect (Patel and Tam, 1981), (Zhao and Zuomin, 2002).

the sample. Resonance in the measurement cell can be utilised to maximise the signal, introducing boundary condition dependence. Because of this, and because the technique suffers from thermal diffusivity, most modern PA techniques use pulsed excitation. In pulsed PA, a high power light source is used with a low duty cycle (Zhao and Zuomin, 2002). Thermal diffusivity has not been a problem in this project.

The conversion efficiency of optical energy in the thermal expansion mechanism is below 10^{-4} in liquid media, which is sufficient sensitivity for PA detection (Zhao and Zuomin, 2002)

Solids have a high absorption coefficient, and the acoustic signal that is generated can be considered a point source. However, the particles in the sample will arrange itself differently than for a liquid sample, and the macroscopic state of the sample will affect the results. In 1999, Jiang showed that single particle samples increased the signal to noise ratio, and the improving factors were reducing the sample cup volume, concentrating the incident light on the sample, and improving the thermal isolation of the sample cup. PAS on very small sample quantities is called microspectroscopy. Jiang's results showed a signal-to-noise ratio (SNR) for a single particle to be more than twice that of a small cup sample. A large cup sample gave worse results.

2.2 Optical setup

2.2.1 Light source

When choosing a light source, considerations have to be made concerning which properties the light source should have. To minimise noise in the PA signal, the light should have stable power and wavelength. Although Bell's experiment was performed using sunlight, the accuracy desired from our experiment makes lasers the prime candidate.
A laser is a light emitting device whose light is highly coherent and polarised. The light has these properties because it is emitted through stimulated emission. In stimulated emission, an incident photon of a certain wavelength causes an exited electron, with excitation energy corresponding to the wavelength of the incident photon, to release the energy in the form of a photon. Electrons are exited through a process called pumping. The photons are reflected between two mirrors, amplifying the stimulated emission effect. One or both mirrors partially transmits laser light that can be coupled to an optical fibre or be released into free space (Nguyen, 2010).
Lasers can be sorted into categories where some of the most common are gas lasers, solid-state lasers, and semiconductor lasers. Different lasers have different operating and power ranges. The more powerful the laser is, the stronger the PA signal will be. Some of the PA literature describe lasers with a power output of more than 100 mW. In many cases such a powerful laser would destroy the sample, which obviously is unwanted since one of the advantages of PAS is that it is non-intrusive. Among the lowest laser powers used in PA is Kosterev et al.'s 1.6 μm DFB diode used in 2002 when conducting measurements on methane. The laser power was 2 mW. Grossel et al. used a 3 mW DFB QCL in 2007 when detecting NO and H_2O bands (Michaelian, 2010).
According to the aim of this project, a laser with the wavelength corresponding to a CO_2 band, ideally not disturbed by H_2O bands must be chosen. The PA signal for CO_2 at the 2004 nm wavelength is about two orders of magnitude larger than the signal at 1573 nm. The strong absorption means that a less powerful laser can be used. This means less hazardous instrumentation, less laser training before use, and thus easier to commercialise and apply in everyday industries. Ultimately, what we want to develop is a small and

compact easy to use and reasonably priced CO_2 detector. These arguments makes the use of a Laser Diode (LD) a good choice.

A diode consists of a n-type and a p-type semiconductor joined together. The area where the n-type and p-type material meet is called the p-n junction, and is the place where the electrons and holes recombine, forming an insulating layer. When forward biased, additional electrons and holes are recombined, resulting in a release of energy. In the case of light emitting diodes (LED), this energy is released in the form of photons by spontaneous emission. The laser diode is a LED where the p-n junction is placed between reflecting mirrors, creating a laser cavity of the p-n junction. Electrons are pumped by the current flowing through the diode. The drive current has to be sufficiently high to overcome optical losses in the laser cavity, i.e. a sufficient amount of electrons must be exited for stimulated emission to dominate. Assuming a certain threshold current, the LD behaves as a LED below the threshold, where the light is not highly coherent.

In this project the nanoplus 356-2004-2 2004nm DFB laser is used. The laser data sheet is included in the appended CD. A distributed feedback (DFB) laser, is a laser where the laser cavity is formed by a diffraction grating on at least one of the sides of the cavity. The grating is designed to reflect only the desired wavelength, making it resonate in the cavity. Changing the temperature causes thermal expansion in the grating, and the refractive index also changes with temperature. Therefore, the wavelength of the laser can be slightly modulated by varying the temperature of the LD. Varying the current will also change the wavelength.

To minimise the error caused by temperature fluctuations, the temperature of the LD must be closely monitored and controlled. The drive current must also be sufficiently accurate and stable. This is achieved using a laser diode driver (LDD) and a temperature controller (TC). Modulation can be performed on the output current of the LDD which goes to the laser. The LDD can have an internal modulation source or it can accept an external analogue voltage. The voltage is converted to output current with a given ratio. Both the temperature controller and the LDD values can be adjusted before they are turned on, to make sure the laser is not overloaded. A current delimiter can also be set, ensuring the current sent to the laser never exceeds the maximum current of the laser.

A common way of measuring the temperature of the laser is using a thermis-

tor. The resistance is set with regards to the desired temperature by using the R vs. T equation for thermistors:

$$R = R_0 e^{(\frac{\beta}{T} - \frac{\beta}{T_0})} \tag{2.11}$$

R_0 is the resistance measured at T_0. β is the thermistor material constant, and T is the desired temperature. The current is controlled by a PID controller, for optimal stability. The temperature controller is in this project used to control the wavelength of the laser.

2.2.2 Optical fibre and polarisation

Electrical signals are transported between components using metal wires. Optical signals, like the laser light described above, must be transported in cables designed to transport light. These cables are called optical fibres and has become increasingly common the last few decades. Optical fibres has low loss, low bit error rates, small and light weight, bi-directional and immune to em-radiation. There are many different types of optical fibres, suitable for different applications. However, they all consist of a core with a certain refraction index, and a cladding surrounding the core with a lower refraction index. The change in the refraction index ensures total internal reflection so that the light stays in the core and does not leak, given that it is sent into the fibre within an acceptance entrance angle. This is illustrated in figure 2.4.

The light from the laser is polarised, i.e. all the electric field vectors lie along the same plane. If the fibre is subject to stress such as pinching or bending, it causes a small change in the refraction index at the point where the stress is applied. This again leads to a change in the polarisation of the light. The measurement cell used for CO_2 detection in gas has a window where the laser light enters the cell. To achieve maximum PA signal, no light should be reflected by this window. This is achieved by mounting the window at the Brewster angle. For a Brewster window, the reflected light is at an angle of 90^o with the transmitted light. If the incoming light has a particular polarisation it results in all the light being transmitted, and none reflected. Figure 2.5 illustrates the Brewster angle. This means that if the fibre is applied just the right stress, the polarisation can be manipulated to ensure

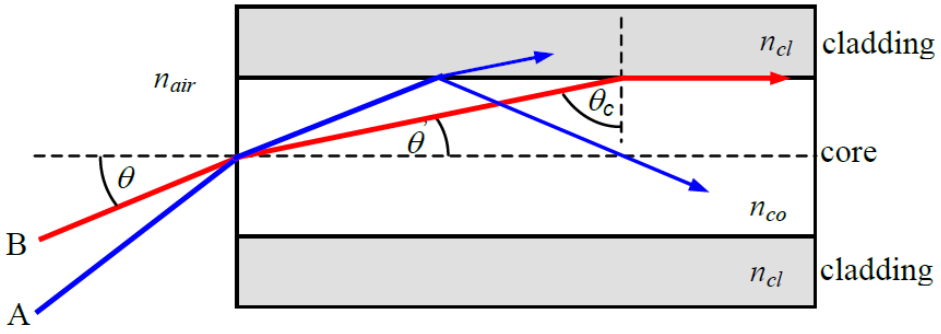

Figure 2.4: Illustration of total internal reflection (Nguyen, 2010).

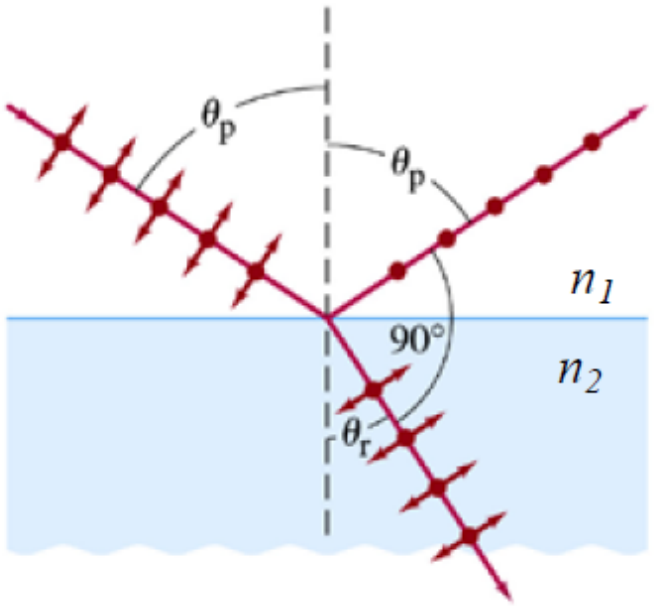

Figure 2.5: Illustration of Brewster angle (Nguyen, 2010).

that all the light is transmitted into the measurement cell. A Brewster angle window is not necessary for the measurement cell used for CO_2 measurements in water, because water has a refraction index similar to glass, and will not reflect a significant amount of light.

2.2.3 Collimation.

To get the laser light into the measurement cell, it must emit from the fibre into free space. When the light comes out of the fibre it spreads at a certain angle. To ensure that as much light as possible enters into the measurement cell, the light must be collimated. This is done using a lens as illustrated in figure 2.6.

2.2.4 Optomechanics

Once the laser beam has been directed from the LD through the optical fibre and into free space using a collimator, it needs to be directed through the measurement cell. In order to achieve best possible PA measurements, it is important that the light passes directly through the centre of the measurement cell, and do not reflect off the measurement cell wall. That may cause reflections and interference, which will complicate the composition of the PA signal. For the water measurement cell, reflections are not a problem because the beam will dissipate very quickly. The gas measurement cell is equipped with a back window at the Brewster angle, to ensure that the remaining light, i.e. the light that has not been absorbed, can escape freely without causing unnecessary reflections. By placing a power meter or an IR-plate at the rear end of the measurement cell, the distribution of the intensity/power should give an indication of whether the beam is hitting the measurement cell walls or not; the beam will not be neatly collimated if it does.
The laser beam is directed using finely tuned optomechanical equipment. The components are mounted firmly onto an optical table or plate. The collimator is fastened to a holder that can be adjusted in the horizontal and vertical direction. The construction should be sufficiently stable so that adjustment of the tilt of the laser is unnecessary. Mirrors can be used to redirect the path of the laser. Other components may be added if needed, like a stress inducing

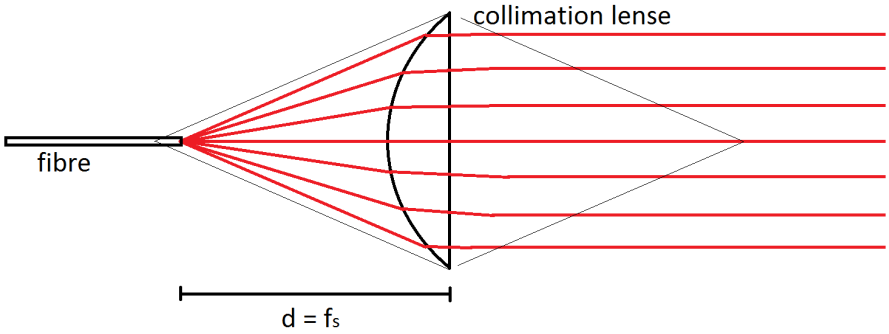

Figure 2.6: Illustration of the collimation principle.

structure for polarisation control, or polarisation filter for investigating the direction of the polarisation.

2.3 Acoustic setup

2.3.1 Sound detection

Obviously, there is a wide range of instruments to choose from when selecting a transducer to measure the acoustic signal. The transducer must be chosen with regard to its frequency response, sensitivity, pick-up pattern and size. Considerations must also be made to ensure a strong output signal by pre-amplifying the transducer signal when necessary.
As an example, an electret condenser microphone will be described in this section, which is the microphone used for the detection of CO_2 in gas in this project. A condenser microphone uses the principle of electrical capacitance. A diaphragm is stretched a distance d from a back plate, see figure 2.7. The diaphragm either consists of, or is coated by a conducting material, and together with the back plate it forms the two plates of a capacitor. Between the electrodes there is a fixed voltage bias of up to a few hundred volts. The capacitance of the condenser microphone is given by:

$$C_0 = \frac{\epsilon_r \epsilon_0 \pi a^2}{d}$$

ϵ_0 is the dielectric constant for vacuum and ϵ_r is the relative dielectric constant for the medium between the plates. When exposed to a sound wave, the diaphragm will vibrate, changing the distance d, and thus the capacitance of the microphone. This change can be measured.

An electret condenser microphone is in many ways an improvement of the regular condenser microphone. The voltage bias in a condenser microphone leads to a charge $q_0 = C_0 V_{DC}$ across the condensator. Because of this relationship, a high voltage bias creates a high charge across the condensator, making small changes in the capacitance due to the vibrating diaphragm harder to detect, i.e. the sensitivity is reduced with increasing V_{DC}. An electret is a material with a permanent polarisation. It can be placed between the diaphragm and the back plate, either as a separate membrane or as a coating to one of the electrodes. Because it has a permanent polarisation, it eliminates the need for a voltage bias. Electret condenser microphones have a high sensitivity over a large frequency range. These microphones normally include an integrated pre-amplifier which provides impedance matching cir-

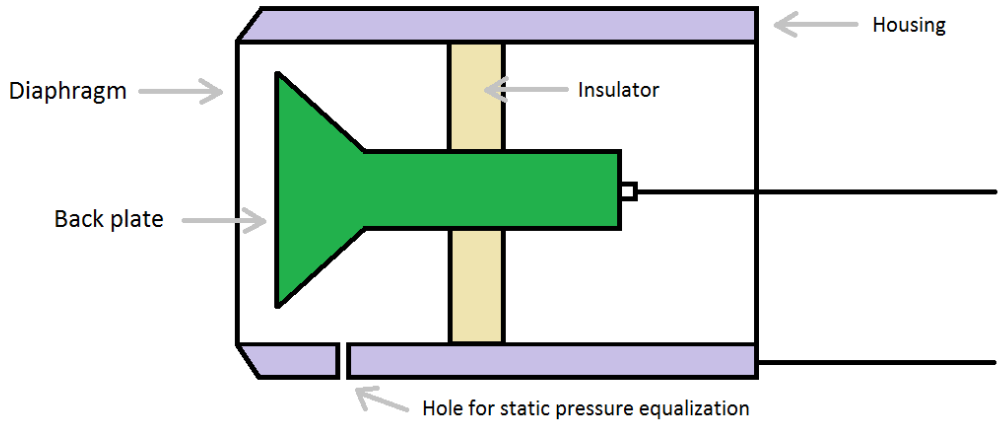

Figure 2.7: Illustration of a condenser microphone.

cuits and gain. (Vestrheim, 2003).

A hydrophone is basically a microphone designed to be used under water. Most hydrophones are based on a piezoelectric transducer, including the one used in this project. The acoustic impedance is designed to match that of water which has a higher density than air. In the project we have acquired a *Brüel&Kjœr* miniature hydrophone type 8103. The directivity pattern of 8103 is shown in figure 2.8. The expected signal from the hydrophone can be calculated. First the conversion from optical power to acoustic pressure must be made. Then the output signal from the hydrophone is simply $Vout = G*p$ where p is the pressure and G is the hydrophone gain. $G = 25.3\ \mu V/Pa$ for the 8103 hydrophone. The power P is equal to pvA, the particle velocity is $v = p/Z$ and the acoustic impedance $Z = c\rho$ for planar single frequency waves. c is the speed of sound and ρ is the density of the medium in question. $A = 4\pi r^2$ is the surface area of the expanded wave. All this put together gives

$$p = \sqrt{\frac{Pc\rho}{4\pi r^2}} \tag{2.12}$$

The highest power likely to get emitted from the LD is $P = 2.0\ mW$. For water, $c = 1500\ m/s$, $\rho = 997\ kg/m^3$ and r is the distance from the source to the hydrophone. For the water measurements cell, which will be described later, this distance is either 6 or 12 cm. Inserting the right values into equation 2.12, the expected maximum signal from the hydrophone is 7.7 mV for the 6 cm cell and 3.9 mV for the 12 cm cell. Realistically however, the PA

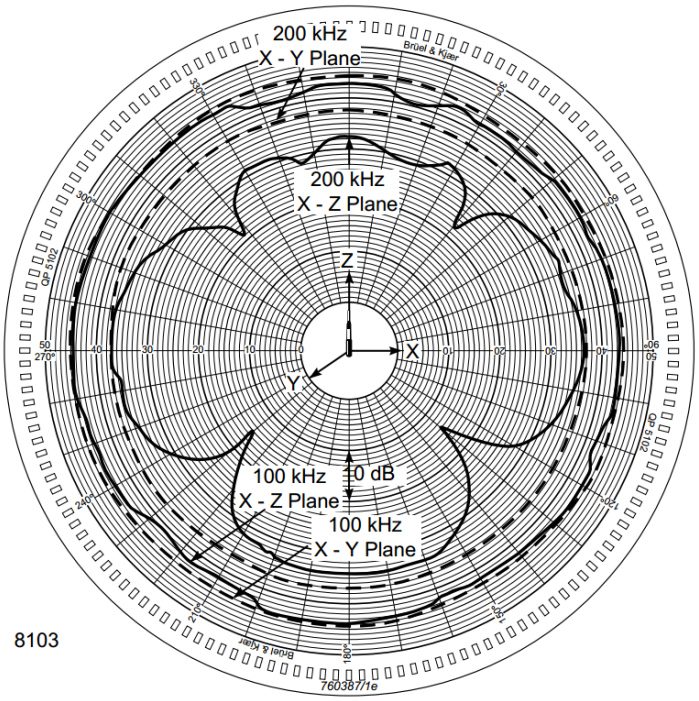

Figure 2.8: Directivity pattern of *Brüel&Kjœr* type 8103 hydrophone.

signal will be much lower than this due to dissipation and losses.
Piezoelectric transducers (PZT) have been used in PA just as long as microphones, however not to the same extent since they are not equally commercialised. The sample can be fixed to the surface of the piezoelectric crystal, eliminating the path the signal would otherwise have had to travel. It is a convenient configuration for solids and it also works very unproblematic in liquids. Ideally it would be nice if a strong, stable, and accurate PA signal could be achieved using a simple and cheap PZT.
An alternative way of measuring the acoustic signal is to use a cantilever optical microphone developed by J. Kauppinen and co-workers (Kauppinen et al., 2004). The cantilever microphone is not limited in the same ways as the capacitative microphone. It is not subject to mechanical damping due to airflow between the membrane and the electrode, it has higher sensitivity, and it is thermally stable. Also, the cantilever bends but does not stretch, making its movement up to two orders of magnitude greater than the tightened membrane of a capacitative microphone. This high sensitivity enables it to measure lower concentrations. It is also linear over a wide range (Michaelian, 2010).

2.4 Other setup

2.4.1 Lock-In Amplifier

The lock-In Amplifier (LIA) is an instrument that uses phase sensitive detection to measure small signal amplitudes buried in noise. It can detect signals as small as a few nano volts buried in noise thousands of times larger. Because the signal received from the acoustic transducer is so small, the LIA is included in the PA set-up. Figure 2.9 shows a simple block diagram of a LIA.

The LIA requires a reference frequency. In our case, the frequency can be obtained from the function generator controlling the current to the laser. The reference voltage is $V_r sin(\omega_r t + \theta_r)$ and the signal voltage is $V_s sin(\omega_s t + \theta_s)$. ω_r and ω_s is the reference and signal frequencies, and θ_r and θ_s is the reference and signal phase respectively. V_r and V_s are the reference and signal amplitudes, respectively. In the LIA, the two signals are multiplied to make V_{PSD}.

$$\begin{aligned} V_{PSD} &= V_s V_r sin(\omega_s t + \theta_s) sin(\omega_r t + \theta_r) \\ &= \frac{1}{2} V_s V_r cos([\omega_s - \omega_r]t + \theta_s - \theta_r) \\ &\quad -\frac{1}{2} V_s V_r cos([\omega_s + \omega_r]t + \theta_s + \theta_r) \end{aligned} \tag{2.13}$$

The output signal has the same frequency as the reference signal, assuming that the reference is obtained from the function generator which also controls the laser which produce the PA signal. Equation 2.13 is therefore reduced to a signal with a constant term $\frac{1}{2} V_s V_r cos(\theta_s - \theta_r)$ and a time varying term $\frac{1}{2} V_s V_r cos(2\omega t + \theta_s + \theta_r)$ The signal is then passed through a low pass filter. The time varying term is thus eliminated. The phase of the reference can be adjusted in the LIA, to make $\theta_s - \theta_r = 0$. The only term left in the signal is then:

$$\begin{aligned} V_{PSD} &= \frac{1}{2} V_s V_r cos(\theta_s - \theta_r) \\ &= \frac{1}{2} V_s V_r \end{aligned} \tag{2.14}$$

V_{PSD} is therefore proportional to the amplitude of the measured signal.

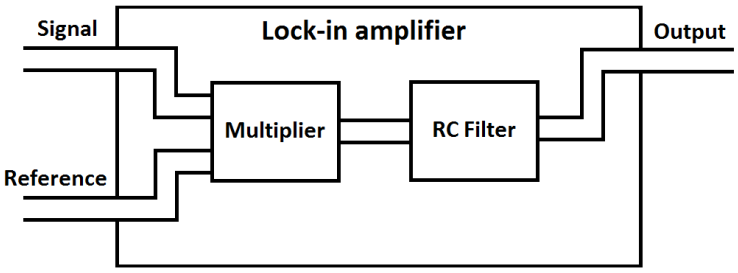

Figure 2.9: A very simple block diagram of the principle of the lock-in amplifier

Suppose the measured signal is not a pure sine wave, but has noise added to it. The filter will only allow frequencies very close to the reference frequency to pass through. Neither $(\omega_{noise} - \omega_r)$ nor $(\omega_{noise} + \omega_r)$ are generally close to 0. Only noise frequencies very close to the reference will be able to pass through the filter. The time constant τ of the filter and the roll-off determines the attenuation of the AC signal. τ should be chosen high enough and the roll-off steep enough to give an acceptable signal-to-noise ratio (SNR).
The dynamic reserve is the ratio of the largest tolerable noise signal to the full-scaled signal expressed in dB. The dynamic reserve changes with the sensitivity/gain. The sensitivity should be chosen large enough for the ADC noise not to be a problem, but not so large that the output signal saturates. The output voltage is limited by the supply voltage of the LIA.
There are two ways to multiply the reference signal and the measurement signal. It can be done with an analogue PSD, or with a digital PSD, by using an analogue to digital converter (ADC). The digital PSD has advantages over the analogue PSD since the analogue PSD have challenges with the following (Stanford Research Systems, 2012):

- Harmonic rejection: When multiplying the reference signal and the measurement signal in the analogue case, the signal will also be multiplied by the reference harmonics. Because the digital PSD reference is computed to 20 bits of accuracy, the harmonics is at the $-120\ dB$ level, thus not noticeable.

- Output offset: The analogue multiplication of the reference signal and measurement signal could contain an output offset. This problem is eliminated by using a digital multiplier. The digital multiplication is

virtually error free.

- Limited dynamic reserve: The dynamic reserve of an analogue system is limited by an error caused by non linearity in the multiplication. In a digital system it is limited by the quality of the ADC.

- Gain error: Analogue sine wave generators are susceptible to amplitude drift, which will directly affect the gain. The digital reference amplitude does not drift.

2.4.2 Measurement cell

The design of the measurement cell varies greatly throughout the literature, depending on the sample at hand. It also varies on the absorption coefficient of the sample, which is why there are two different cells in this project. One for detecting CO_2 in gas and one for detecting CO_2 in water.

Measurement cell for gas detection

Bijnen wrote an article in 1996 called "Geometrical optimization of a longitudinal resonant photoacoustic cell for sensitive and fast trace gas detection". The measurement cell described there has been the inspiration for the gas-detection cell in this project. It consist of a resonator placed between two buffers, all made of stainless steel. Figure 2.10 shows a photo of the PA measurement cell for gas detection. At the end of the buffers there are windows positioned at the Brewster angle. The Brewster angled windows are chosen over anti reflection (AR) coated windows because AR windows reflect radiation, causing more reflections in the buffer, and ultimately increasing the PA signal from the walls.
The resonator radius r_{res} is preferred small, as this yields a higher cell constant. However, a too small radius causes high PA background signals due to absorption of the wings of the Gaussian laser beam profile. To distinguish the gas absorption signal from the signal originating from the walls, windows, and interfering gas, the laser can be switched to other laser lines for a reference signal. Regretfully, deviation in grating position and thermal

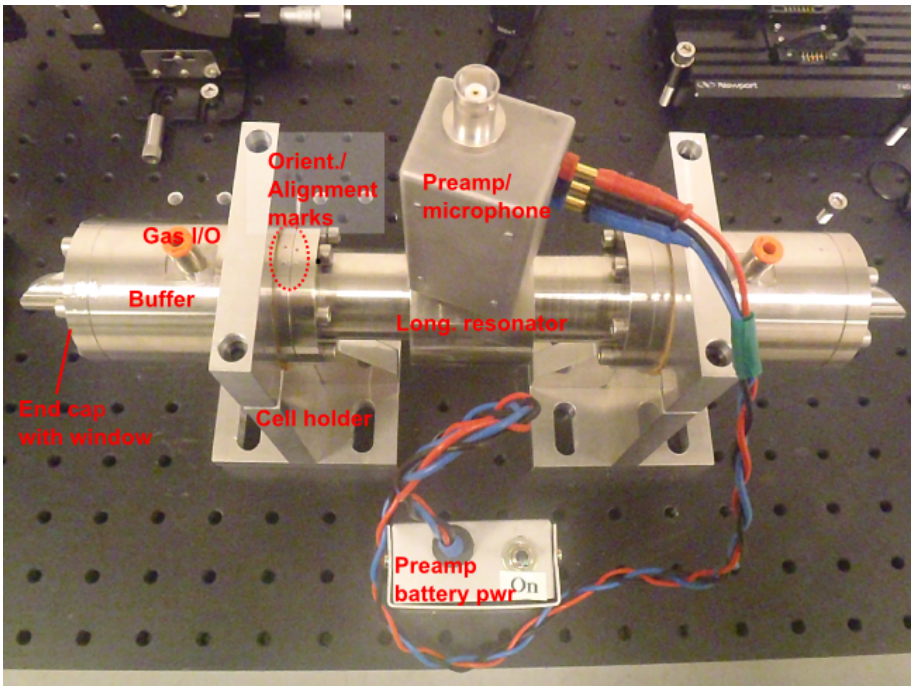

Figure 2.10: The PA measurement cell for gas detection

drift as a result of repositioning the laser beam makes the absorption signal irreproducible, ultimately contributing to the detection limit.

Bijnen showed that a larger buffer radius r_{buf} resulted in a larger measurement cell constant and a lower window signal. Considering the buffer length l_{buf}, the best attenuation was found at $\lambda/4$, the optimal length for destructive interference for pressure amplitudes introduced into the buffer from either one of the sides (Bijnen et al., 1996). Optimal window signal suppression was found for $l_{res} = 2l_{buf}$ where l_{res} is the length of the resonator. The signal amplitude is barely affected if $r_{buf} \approx 3r_{res}$, although a radius this big might not be practical for all applications.

The positioning of the gas inlet also affects the PA signal if continuous flow is needed. The microphone is placed at the centre of the resonator where the signal is as far away from the noise in the buffers as possible. For a fast response, the gas inlet should be close to the microphone, but this will introduce flow noise. Flow noise can be minimised by keeping the flow at a minimum. Alternatively, the gas inlet can be placed in one of the buffers, decreasing the noise at the expense of the response time. A compromise must be made concerning the radius of the gas inlet tube. A small radius is needed to avoid letting in external noise, although this will again decrease

the response time.
The length of the resonator determines the resonance frequency f_{res}. The resonance frequency ω of a fully open resonator is given by

$$f_{res} = \frac{c}{2l_{res}} \tag{2.15}$$

also

$$p_g \propto \frac{\sqrt{l_{res}}}{r_{res}}[1 - \frac{r_{res}^2}{r_{buf}^2}] \tag{2.16}$$

where p_g is the gas absorption pressure amplitude. Inserting eq. 2.15 into eq. 2.16 we see that $p_g \propto 1/\sqrt{f_{res}}$. For frequencies below 1 kHz, the $1/f$ amplifier noise becomes an issue. Above 1 kHz, the frequency independent Brownian noise is the main source of noise. A resonance frequency between $500 - 1500$ Hz corresponds to approximately 10 $cm < l_{res} < 30$ cm. From eq. 2.16 we see that the signal is stronger for larger l_{res}. However, the time response demands a shorter measurement cell (Bijnen et al., 1996).
Based on this, the longitudinal resonator was determined to have an internal diameter of 6 mm and a length of 120 mm. The buffers on each side of the resonator are 60 mm long each with 20.5 mm radius.

Measurement cell for liquid detection

The drawing for the measurement cell used in the water measurements is shown in figure 2.11. Water has a much higher absorption coefficient than air. As mentioned earlier this makes the sound propagate spherically, and the hydrophone can be mounted on the back of the cell. The cell must be sufficiently long for the waves to be plane by the time they reach the hydrophone. To calculate how far from the source the hydrophone must be placed for the sound waves to be considered plane, consider the illustration given in figure 2.12. For plane waves $sin(\theta) = tan(\theta)$. or $x/r = x/r'$. The difference between r and r' must be below a certain tolerance for the waves to be plane. The length of the measurement cell must be decided based on this tolerance. That is why two measurement cells for water detection were made. $x = 9$ mm is the width of the hydrophone used. Using $r = 6$ cm gives $r' = 6.067$ cm, so the tolerance must be below 0.67 mm. For $r = 12$ cm, $r' = 12.034$ cm and the tolerance must be below 0.34 mm. The

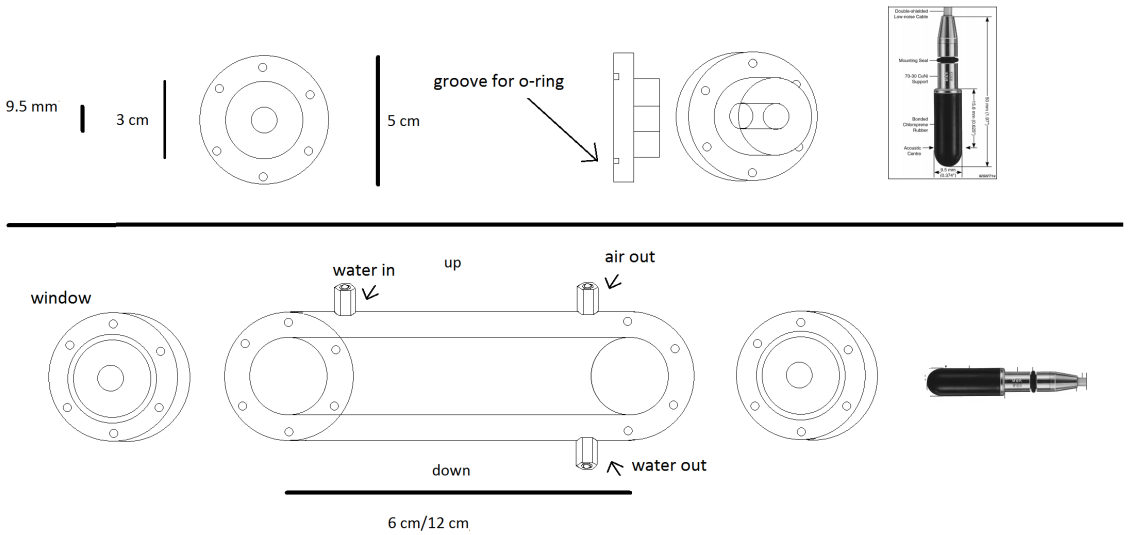

Figure 2.11: The PA measurement cell for water detection

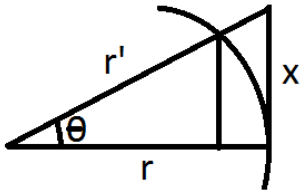

Figure 2.12: Illustration for calculating distance from source for a plane wave approximation.

problem is that the exact tolerance is not known so both cell lengths will be tested. A longer measurement cell is not tested because the sound signal will be attenuated and might be to weak to detect if the cell is too long. The measurement cell also has an inlet and outlet for the water and an outlet for excess air.

2.4.3 Gas flow controlling equipment

In order to calibrate the PA equipment, the CO_2 concentrations must be known. Achieving that can be done in a number of ways. Three alternatives were considered. Firstly, a separate CO_2 detector could be used. Victoria University acquired a Dräger X-am 5000 CO_2 detector. Unfortunately, the

detector was very coarse, measuring concentrations from $0-5\%$ with no decimal points. Finding a detector that has a sensitivity and operating range that can match the PA technique is difficult and expensive. In addition, having a sensor is not the same as being able to control the concentration. The second alternative is therefore to buy premixed gas. In premixed gas, the exact concentration is known, and need not be measured. Ideally, this would be the best alternative, because it is the most accurate one. But premixed gas is unfortunately quite expensive, especially in this case where many different concentrations are desired. This leaves the third alternative: Mixing gas using N_2, CO_2 and flow controllers. This alternative is a compromise between economy and accuracy. Figure 2.13 show a picture of the gas-mixing equipment used in this project. Two Bronkhorst EL-FLOW Select Mass flow controllers were used, one calibrated for N_2 gas, and the other for CO_2 gas. The two gases are mixed after flowing through the controllers separately, by joining the tubes in a T-junction.

2.4.4 Data acquisition

The PAS technique called PA Fourier-transform infra-red (FT-IR) spectroscopy will now be described. This is not the technique used in this project, but is included because it is often used and should be mentioned. In PA FT-IR spectroscopy, there are two ways of performing the scan. It can be done either by rapid-scan or step-scan. A PA FT-IR spectrum obtained using rapid-scan may need normalisation. A background spectrum can be obtained by measuring the spectrum of the empty measurement cell. The signal generated from an empty measurement cell is caused by the optical and electronic characteristics of the measurement cell and microphone. In solid state PAS, the "empty" sample is often powdered carbon black, glassy carbon or carbon-filled polymers. For gas PAS, inert gas can be used, e.g. N_2. The laser in the experimental setup of this thesis can be tuned between approximately 2000 nm and 2006 nm, which is not a very wide range. It is fair to assume that normalisation in this case is not necessary. Step-scan measurements involve the use of a constant modulation frequency. The spectra has not wavenumber-dependent frequency effects like the rapid-scan method has. This makes the step-scan spectra a closer approximation to ordinary ab-

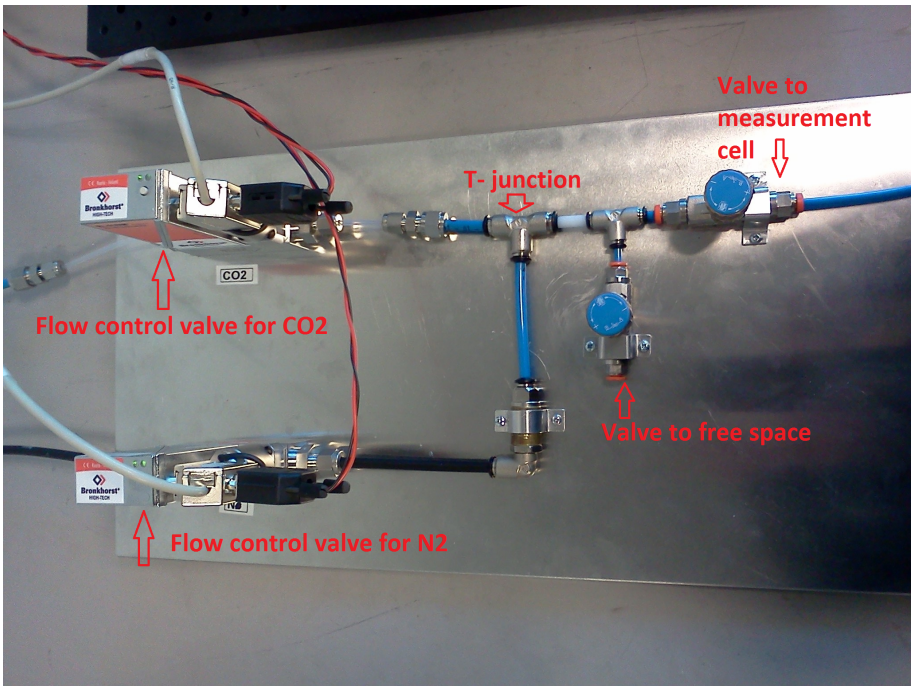

Figure 2.13: Flow controllers mixing the gas

sorption spectra. The step-scan FT-IR PA is advantageous because it gives better results in depth profiling, the use of the phase spectrum extends the dynamic range.

Originally, a lock-in amplifier was needed for signal recovery in a step-scan PA experiment. A lock-in amplifier is still being used in many PA experiments, but digital signal processing (DSP) demodulation has now made it possible to recover the signal using software only. The stepping of the movable mirror in step-scan, amplitude or phase modulation and sampling rate of the analogue-to-digital converter(ADC) are all synchronous, and can therefore construct the sample response to a periodic modulation through two interferograms. The real and imaginary interferograms, corresponding to in-phase and quadrature interferograms from a lock-in amplifier, are obtained. DSP demodulation offer simultaneous signal recovery for several harmonic multiplies of a frequency through Fourier transformation, eliminating the need for repeated measurements, and facilitating depth profiling. At higher frequencies though, the LIA spectrum have better signal-to-noise ratio than a corresponding DSP demodulated spectrum. This is probably due to the sampling rate of the ADC (Michaelian, 2010).

Averaging is important to get reliable results. Factors like background noise

picked up by the microphone will be averaged at least to some extent, and variation in the signal due to gas circulation, and electrical disturbances will also be averaged. Technically, the more samples available for averaging the better. But taking samples takes time, drift in the signal may occur due to heating by the laser, and waiting for the sampling to complete is tedious. A compromise is therefore made.

In this project, a conventional LIA is used. The various instruments in the setup are controlled by LabVIEW using GPIB and USB connections, and the software "Measurement and Automation Explorer" (National Instruments) using RS232 connections. The LabVIEW program that is developed for the PA experiments are described in detail in the next chapter.

Chapter 3

Measuring CO_2 in air

So far, the techniques and possibilities for using PAS has been discussed. Initially, PAS was used qualitatively, which is natural for any new technology. As more research was done on the subject, it was made increasingly clear that PA could be used for quantitative measurements. Ultraviolet and visible PA spectra sometimes showed signs of saturation, making PAS unfit for feasible measurements. However, absorption coefficients towards the IR can be several orders smaller, making it less likely to have saturation towards IR PAS. The focus of this project is to investigate if it is possible to detect CO_2 in water using PA with a 2004 nm slightly tunable LD. Initially the PA signal from gas-phase CO_2 will be investigated. The amplitude of the absorption bands indicate the concentration of CO_2, and by varying the concentration in the measurement cell, the quantitative aspect of the measurement will also be investigated. It is important to demonstrate that PAS can successfully be used for quantitative analysis. An example of a successful quantitative experiment was done by McClelland et al. in 1992. The concentrations for the components in a mixture of coal and three different clay minerals were successfully identified within $1 - 2\%$ accuracy (Michaelian, 2010)
The work of Pandurangi and Seehra in 1992 is an example of where saturation affected the result, making PA unsuited for quantitative measurements for higher concentrations. Measurements were done on silica and silica-kaolin mixtures at 5.3 μm. These two examples show that PA can be used for quantitative analysis, but care must be taken to avoid situations where saturation can be a problem.

3.1 Materials and Methods

Some of the alternatives for the experimental setup was investigated in the previous chapter. In this section, the specific setup of this project will be described.

In the initial version of the experiment performed at Victoria University (Melbourne, Australia), the set-up was as shown in figure 3.1. The laser was a 2004 nm DFB laser from the company nanoplus mounted on a Newport butterfly LD mount. It was controlled by a Newport 350 temperature controller (TC) and Newport 560 laser diode driver (LDD). The LDD was modulated externally by a GW model GFG - 8016G function generator. Because the function generator did not have digitalised amplitude and offset tuning, an oscilloscope was used to ensure that the desired values were achieved. The microphone used to detect the pressure waves was a KE 4-211-2 Sennheiser back-electret condenser microphone connected to Analogue Devices AD797 operational amplifier.

The design for the measurement cell for gas detection was based on the article "Geometrical optimization of a longitudinal resonant photoacoustic cell for sensitive and fast trace gas detection" by Bijnen, Reuss and Harren in 1996. The power meter was a home made device made by senior lecturer Dr. Thinh Nguyen (VU) which was not wavelength sensitive. It was only used for qualitative measurement related to alignment of the laser, in addition to an IR-plate. Finally, the LIA used was a type Femto LIA-mv-150, which is analogue, and was connected to an oscilloscope.

In later experiments performed at UIB, the same measurement cell, laser and microphone was used. This time, a Thorlabs ITC4005 laser diode/ temperature controller was used with a Thorlabs butterfly LD mount. Unlike the Newport TC and LDD, the Thorlabs TC and LDD is incorporated into the same physical device. This offers extra operational security, since the laser can not be turned on unless the TC is on. Finding the right PID control parameters is also easier on the Thorlabs device. Even though the ITC4005 has an internal modulation function, an Agilent 33500B waveform generator was used for external modulation. Stanford Research Systems SR850 DSP LIA was used with the Agilent 33500B as reference frequency. The waveform generator and the LDD/TC were connected using a USB cable to the PC via a USB hub. The LIA was connected to the same USB hub using a GPIB-

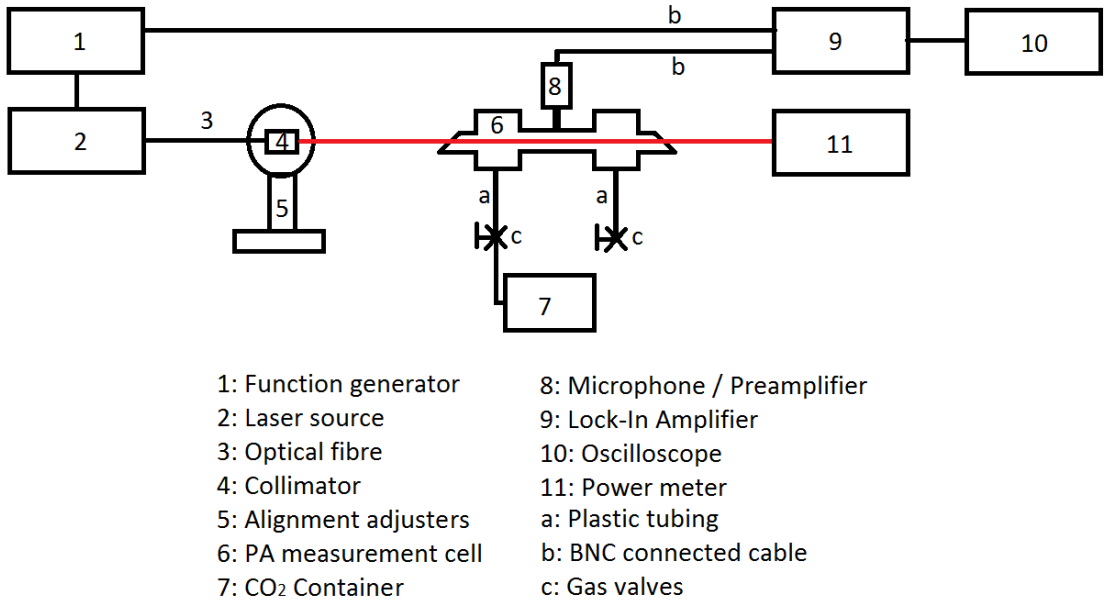

Figure 3.1: Initial PA set-up.

USB cable. From the PC, the equipment was controlled using LabVIEW. To be able to accurately adjust the CO_2 concentration in the measurement cell, a N_2 tank and a CO_2 tank were each connected to a separate Bronkhorst High-tech EL-FLOW MBC3 flow controllers. The controllers were managed using the "Measurement and Automation Explorer" software by National Instruments on the PC via RS232-USB cables. Valves and metal joints were used to direct the gas into the measurement cell. The optomechanical devices used were from Thorlabs, and a Thorlabs PM-100D power meter was used to investigate the laser characteristics. The optical fibre was coiled to control its polarisation, and checked with the power meter and a linear polarisation filter. This new experimental setup is illustrated in figure 3.2, and includes the gas flow setup and the PC interface connections. The different types of cable are shown by different colours.

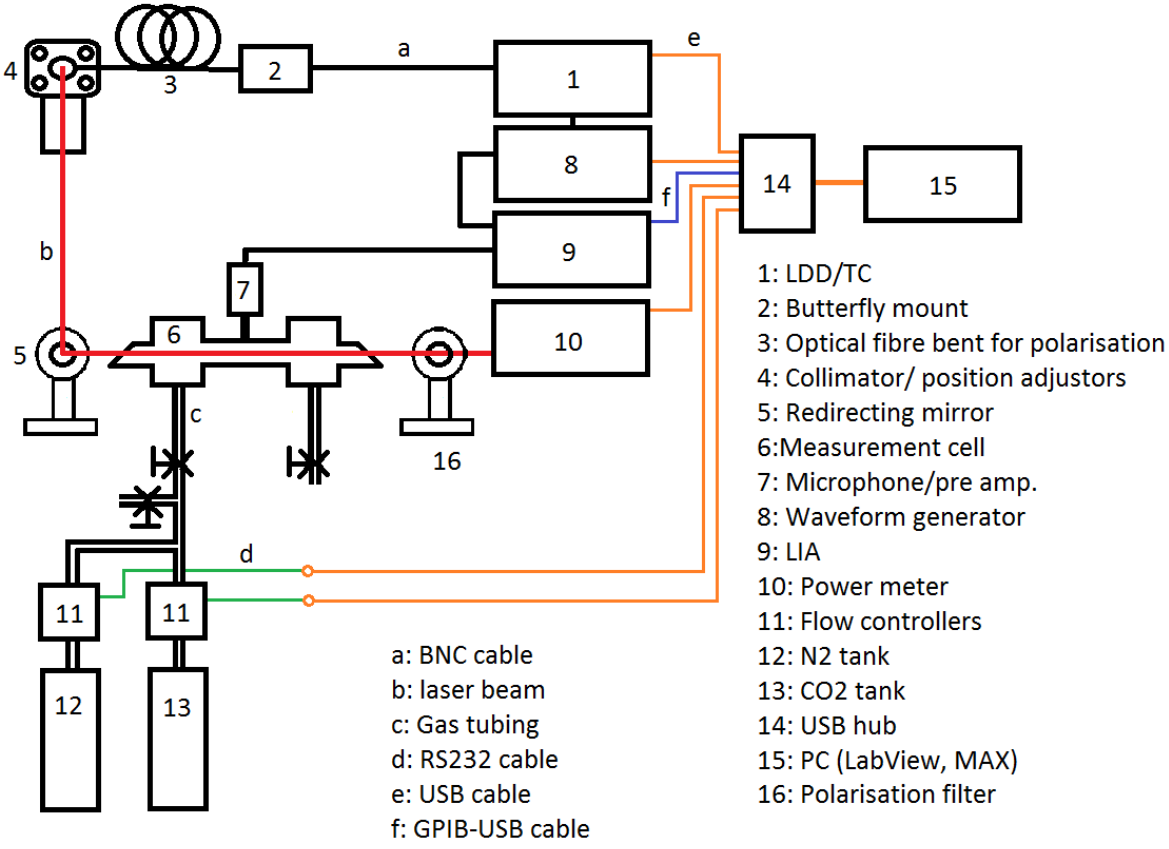

Figure 3.2: Final PA setup at UIB.

3.2 Experiments

3.2.1 Basic initial experiment

Motivation

Before presenting the quantitative results of the experiments, it is important to know that the equipment used is reliable, and that it is actually performing in the desired way. For example, turning on the laser prior to the temperature controller (TC) may result in laser overheating, and possibly destroy it. It is important to know how the components in the PA setup work in order to more easily be able to identify and solve errors later. This is why the initial experiment was performed to gain experience and a practical understanding of the PA measurement principle.

Execution

The setup as shown in figure 3.1 was used, and the experiment was performed at the optical laboratory of Victoria University. Initially, the LD needed to be mounted on a butterfly LD mount. The circuits were carefully checked to make sure the thermistor, the TEC anode and cathode, and the LD anode and cathode were correctly connected, using a voltmeter. The temperature of the laser is measured by a thermistor and controlled by a Thermoelectric cooling (TEC) element, and the relationship between the tunable resistor and the desired temperature is given by eq. 2.11. β, T_0 and R_0 are constants given in the data sheet as 3930, 25^o C and 10 $k\Omega$, respectively. The resistance was taken as input for the TEC. The PID parameters of the TEC had previously been set and did not need adjustments. Also, a current limit of 1.9 A had been set. From the data sheet of the laser, the operational range is between $35-45^o$ C. Inserted into eq. 2.11 this yields $R_{min} = 4363\ \Omega$ corresponding to the maximum temperature, and $R_{max} = 6517\ \Omega$ corresponding to the minimum temperature. The laser will not be destroyed for temperatures below the operational range, but it might not lase reliably. Care must however be taken not to overheat the laser. When the temperature was stable, the laser could be turned on. For external modulation, the LDD had a conversion rate of 300 mA/V. The function generator was set to a square wave with $f \approx 1310$

kHz. The laser current amplitude was set according to the relationship

$$out[mA] = 300mA/V * in[V] \tag{3.1}$$

where in is the output voltage of the signal generator. The LD current was modulated between 0 mA and 70 mA. On the LDD, the current delimiter for the LD was set to 120 mA, which is the maximum operating current. Currents higher than this may damage the LD. The optical fibre from the laser was terminated with a collimator, and the beam was aligned through the measurement cell. By using a IR-plate, the beam could be seen coming out of the rear of the measurement cell. The shape of the beam indicated whether it had been reflected and scattered in the measurement cell walls. Combined with a power meter, a good alignment was achieved. The microphone was checked for faulty connections using a voltmeter before it was firmly attached to the measurement cell, and its signal was connected to the LIA. During the measurements, the measurement cell was filled with pure CO_2 gas for a maximum signal. The PA signal from the LIA was observed on an oscilloscope rather than a voltmeter because the oscilloscope can average a larger part of the signal and thus give a more accurate result. The LIA time constant, sensitivity and phase was adjusted. The time constant $\tau = RC$ determines the cut-off frequency. If τ is set too small, more frequencies are let through, and a cosine oscillation could be observed in the filtered signal. When τ was set very large, it took a long time for the signal to stabilise. $\tau = 30$ ms seemed to be a good compromise. The sensitivity setting was found the same way. The sensitivity determines the gain. High sensitivity, and the signal was out of range and thus clipped; too low and the resolution was a problem in addition to a very small signal. The sensitivity was set to $S = 30$ mV. The phase gives zero signal amplitude for two angles 180^o apart, one maximum value at $+90^o$ angle from, and one minimum value at an angle -90^o from one of the zero signal amplitude angles. After these initial steps were taken, a temperature sweep could be taken to see how the PA signal changed as a function of wavelength. As mentioned in section 2.2.1, the wavelength of the laser is temperature dependent, and a temperature sweep is equivalent to a wavelength sweep. Figure 3.3 has been generated using HITRAN database, and show the absorption coefficient of CO_2 in the wavelength range of the nanoplus laser. The laser was specified to have a

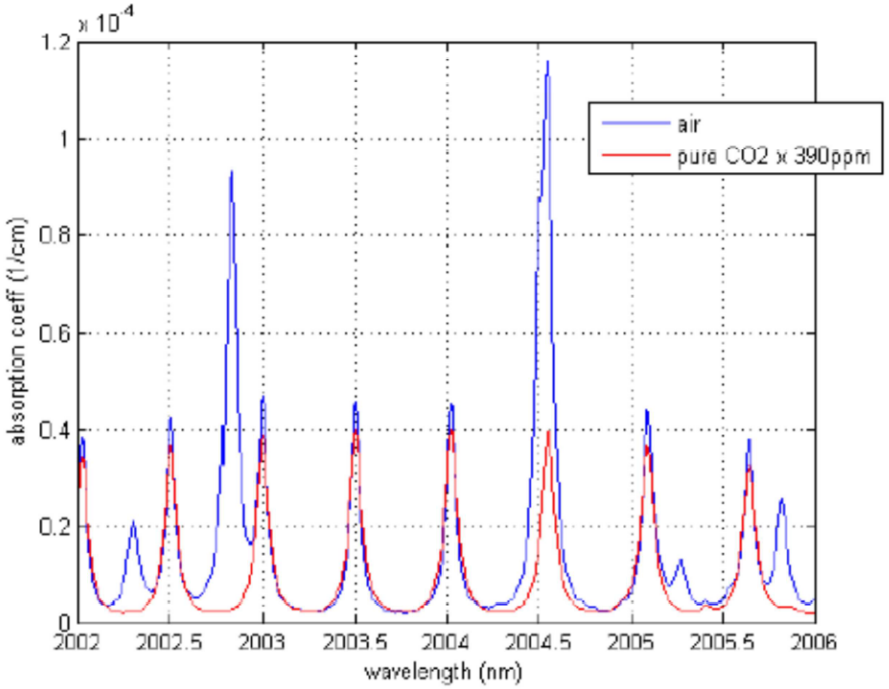

Figure 3.3: Absorption coefficients from HITRAN. The difference between atmospheric air and pure CO_2 is due to H_2O which may vary depending on relative humidity.

range between 2003.7 to 2005.8 nm for the given temperature range. The resulting PA signal is shown in figure 3.4. Although the number of data points is relatively small, it can easily be compared with the absorption coefficient from HITRAN.

The initial set-up had no way of controlling the CO_2 concentration. The concentration was roughly adjusted by filling the measurement cell with inert gas, and inserting one syringe after the other with CO_2 and monitoring the PA signal between each inserted syringe. Furthermore, the measurement cell was filled with CO_2 and syringes of inert gas was added. Even though not very accurate it gave an indication that the PA theory is correct, which was the intention of this experiment. The concentration was calculated based on the volume of the measurement cell, $V = 58 \pm 2\ mL$, and the volume of the syringe. The following equation was used to calculate the concentration a_{CO_2} of CO_2 based on the number of moles of the different gases.

$$a_{CO_2} = \frac{n_{CO_2}}{n_{CO_2} + n_{N_2}}$$

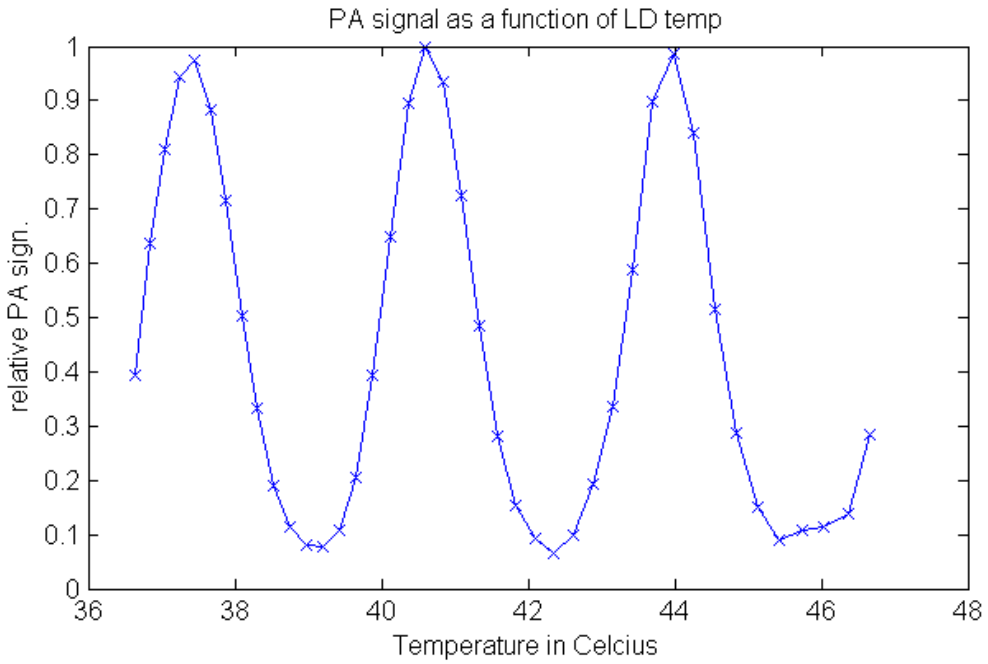

Figure 3.4: First PA sweep, performed at Victoria University. The values of the PA signal are relative.

where the amount of substance n is:

$$n = \frac{PV}{RT}$$

from the ideal gas law. P is the pressure, V is the volume, T is the temperature and R is the ideal gas constant.

Results

The results of the experiments are given in figure 3.5 The same steps were taken when setting up the equipment at UIB, only this time, all the components were plugged to a computer, and the gas was controlled using a gas flow controller. That made the variables of the experiments easier to control and adjust. The advantageous adjustments of variables will be investigated next.

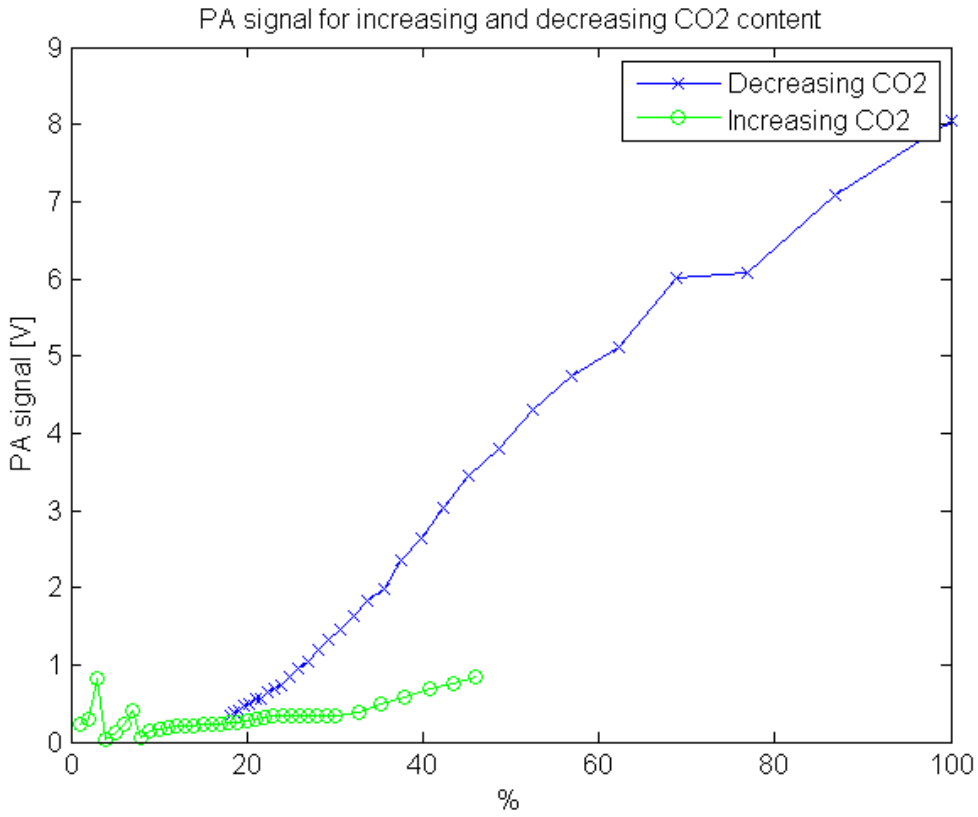

Figure 3.5: PA signal with varying CO_2. The syringe method is not accurate, but the general idea of increasing signal with increasing CO_2 concentration is conserved. The signal seem disturbed at initial data-points for the increasing CO_2 plot.

3.2.2 Amplitude vs phase modulation, excitation frequency and other parameters

Motivation

The rest of the experiments were all performed at UIB. With the equipment being as described in figure 3.2. In this section, three main issues will be addressed. First, regarding the waveform generator, two different types of modulation will be presented. Second, with regard to the geometric shape of the cell, the modulation frequency will be discussed, and third, the importance of correctly tuned parameters for the LIA will be discussed.

Execution

Signal modulation can be achieved through various methods. The oldest technique is by using a chopper, the way Bell did in his original experiment in 1880. Even though it is old, it is still an acceptable way to modulate the laser beam. It provides a good square wave signal, and the power of the light is kept constant. The laser can also be modulated by using an external function generator to modulate the current sent to the laser. In doing so, the power may vary slightly, specially if the laser is turned off between light bursts. This is called amplitude modulation. For example, the laser current could oscillate between 10 mA which is below the laser threshold current, and 100 mA which is not far from its maximum current. This is the most intuitive straight forward modulation. A square wave can be represented by eq 3.2 through Taylor expansion.

$$Sq(\omega t) = sin(\omega t) + \frac{1}{3}sin(3\omega t) + \frac{1}{5}sin(5\omega t) + ... \tag{3.2}$$

At each odd harmonic frequency, we expect to see a PA signal. The LIA can be used to find the signal for several harmonics by taking successive measurements or DSP demodulation can be used. The first harmonic provides the strongest signal. Reduced bandwidth in the higher harmonics can however allow identification of some features that were unidentifiable in the first harmonic spectrum.

Amplitude modulation hold some disadvantages. The small changes in power due to the rapidly changing current may cause a significant error in the resulting signal. Only a part of the laser's power is being utilised by having the laser off half the time. This is specially unfortunate considering the nanoplus DFB laser have a very low power in the first place, compared to many other lasers in the literature.

In phase modulation, instead of having a large difference in laser current and thus power, the laser is modulated with a minimally changing current. For example, the current could oscillate between 85 and 95 mA. The spectra of phase modulation looks like the derivative of the amplitude modulated spectrum. The small current variation causes a small shift in wavelength, so the measurements is associated with the formula for numerical derivation.

$$\frac{dS}{d\lambda} = \lim_{\Delta\lambda \to 0} \frac{S(\lambda + \Delta\lambda) - S(\lambda)}{\Delta\lambda}$$

S is the PA signal. Although the actual absorption peaks can not be seen as neatly for phase modulation, it gives a stronger signal, which may come in handy. External modulation also offer a sinusoidal modulation, unlike the chopper which only generate a square wave. Often the LIA has a function generator built in, so the LIA can be used to modulate the current to the laser. This also means that the reference signal is internal for the LIA, and therefore only need the unfiltered PA signal to recover the PA signal. However, in this case external modulation was used. The PA signal for amplitude modulation, phase modulation using square wave and phase modulation using a sine wave were measured with all other parameters remaining constant. This way, the difference in amplitude and shape could be compared.

As for the frequency, choosing it to be equal to the resonance frequency of the measurement cell is not always necessary, but will increase the PA signal. The length of the resonator is what determines it. Resonance is achieved when standing waves are generated i.e. $\lambda = 2l_{res}$, where λ is the resonance wavelength and l_{res} is the length of the resonator. Since $\lambda = c/f$, where c is the speed of sound in a given medium and f is the resonance frequency, the frequency can be written as

$$f = \frac{c}{2l_{res}} \tag{3.3}$$

With $l_{res} = 0.12\ m$ and $c_{air} = 343.2\ m/s$, the resonance frequency is expected to be $f = 1430\ Hz$. To find the resonance frequency experimentally, the cell

was exited externally by a small loudspeaker driven with a sine output from the LIA. The LIA was set to sweep from 1200 to 1500 Hz in 300 seconds with $\tau = 0.3\ s$.
The motivation for fine tuning the time constant and sensitivity of the LIA has already been explained in the previous section. In addition, the sampling frequency and total scan time must be set. The two values multiplied gives the amount of measuring points the LIA eventually returns. The scan time must be large enough compared to the temperature interval, so that the temperature step is small enough for the temperature to settle in the given time for that sample, set by the sample rate. This is further explained in section 3.2.3.

Results

Figure 3.6 shows the amplitude of the three different modulation methods mentioned. We can clearly see the absorption peaks in the amplitude modulation plot. The phase modulation plots looks like the derivative of the amplitude modulation, and the peak is also slightly shifted. The maximum amplitude for the three signals are fairly close, however the phase modulation signals have a slightly higher amplitude as expected. In the further experiments the amplitude modulation will be used because the signal is easier to interpret, and because it is not significantly lower in amplitude.
The resonance frequency is found in figure 3.7. A peak is clearly seen with a maximum at $f = 1310\ Hz$. The FWHM is approximately 70 Hz giving a Q-factor of about 19 for the resonator.
The PA signal for different sensitivity values are as shown in figure 3.8. When air occupies the cell, a sensitivity of $0.01e-3$ is too low, giving no sensible PA signal. A sensitivity of $10e-3$ gives a choppy signal plot, whereas a sensitivity of $100e-3$ obviously is too coarse. For other CO_2 consentrations, the sensitivity may need to be different. PA signals taken with different sensitivities can not easily be compared because the sensitivity setting affect the measured amplitude, as can be seen in plot 3.8.

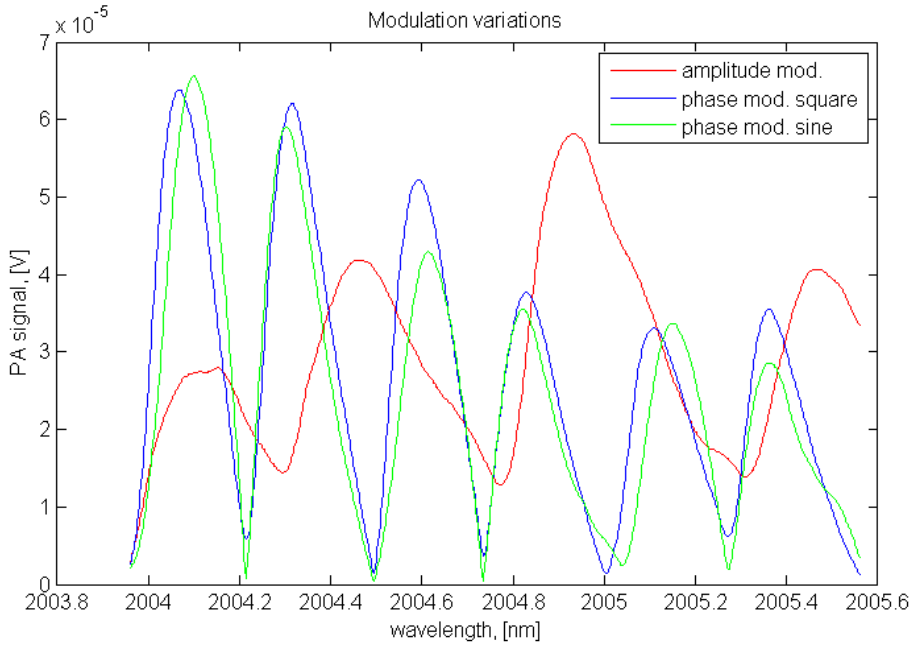

Figure 3.6: Three different ways to modulate the laser. Produced with $f = 1310\ Hz$, $sens = 1e-3$, $timeconst = 3\ s$. The current was $I = 10-100\ mA$ for amplitude modulation and $I = 95-105\ mA$ for phase modulation. The measurement cell was filled with air.

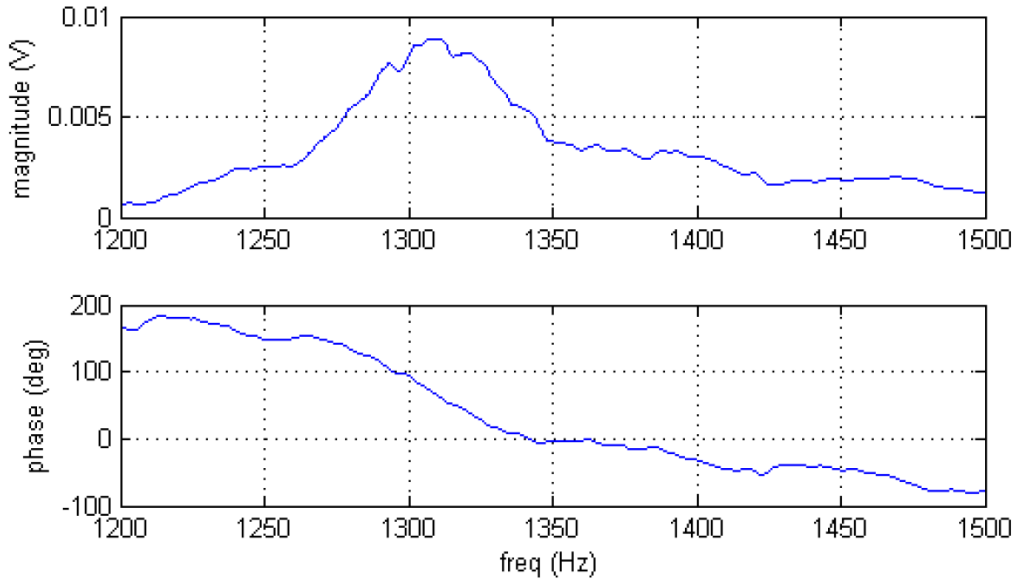

Figure 3.7: Determining the resonance frequency.

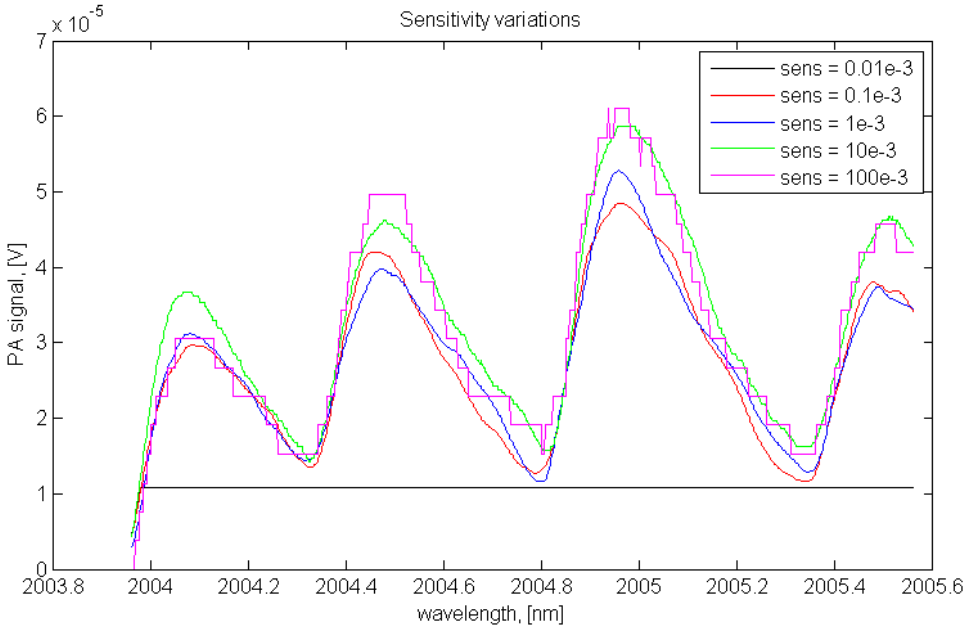

Figure 3.8: Sensitivity of LIA varied.

3.2.3 LabVIEW

Motivation

An automatic sweep over the wavelength range of the LD is faster than doing it manually. LabVIEW eliminates the need for performing repetitive tasks by automating them, making data acquisition much more efficient. The LabVIEW software development tool communicates with many devices simultaneously, it is easy to learn and understand, and it is capable of returning data in a desired form. This section is a description of the LabVIEW program designed in this project to utilise PAS.

Execution

The devices that are controlled using LabVIEW are the waveform generator, the LD/TC controller and the LIA. The flow controllers mixing the gas for the measurement cell were supposed to be controlled using LabVIEW, but due to technical difficulties, they were controlled using the software Measurement and Automation Explorer (MAX) from National Instruments. Before writing the LabVIEW VI, communication was established with each of the

devices using MAX. This way, possible interface communication errors were taken care of initially so that they would not be a problem in a later more complex program.
The LabVIEW VI data acquisition procedure made for this project can be divided into three stages. First, the devices must be initialised and the initialisation parameters set. Second, the data acquisition commences, i.e. the LD/TC controller performs the temperature sweep, and the LIA must record the sound signal. Third, the data is read from the LIA and plotted, and all the devises are turned off and closed.
The waveform generator uses the Agilent 33XXX series library. In the initialisation VI the VISA resource name, frequency, waveform function, amplitude and DC offset is set. A case structure ensures that an acceptable amplitude input is given even if the user sets an amplitude that is out of range, that is less than 0.01 Vpp or larger than 10 Vpp. Figure 3.9 shows the initialisation of the waveform generator.
Figure 3.10 shows the initialisation VI for the LIA. The VISA resource name, sensitivity, time constant, sampling frequency and total scan time is taken as input. One can also choose between internal and external reference input, but this option is always set to external. The inputs are combined in a command string and sent to the LIA using generic VISA-GPIB communication. The traces the LIA should put in the buffer is also defined as the amplitude "R", the phase "θ" and the analogue input 1 and 2 (not used).
Figure 3.11 show the initialisation of the LD/TC controller. The temperature and current limits have already been set manually so they do not need to be set using LabVIEW. The VISA write function is used to set the temperature and turn the temperature controller on. Then the same function is used to set the current and to turn the laser on. A for-loop forces the current commands to wait to be executed until after the temperature has properly stabilised. A wait command is added after the laser has been turned on because the laser turns on 3 seconds after the command is given, and the temperature should have time to stabilise after the laser had been turned on. The wait command after the for-loop is for redundancy. The command for turning on the laser has been placed in a flat sequence structure to ensure that an attempt to turn the laser on will not be executed until the temperature controller is turned on and stable.
This concludes the initialisation part of the program. It is time to start the

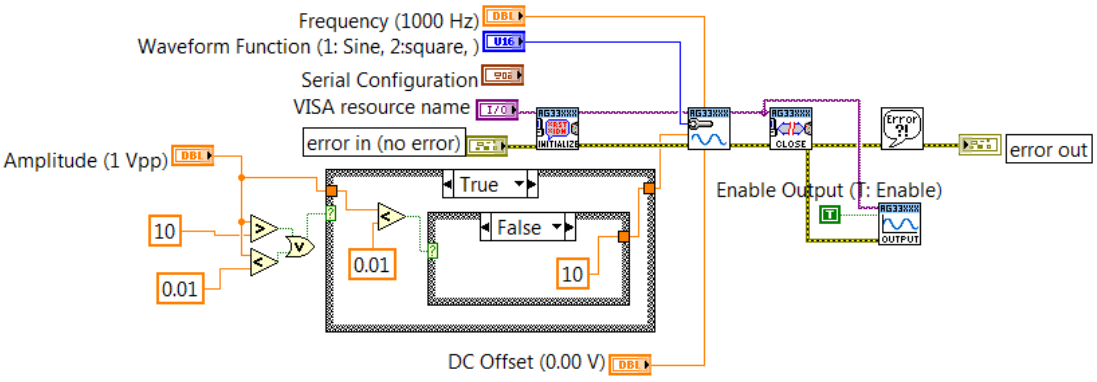

Figure 3.9: Initialising the waveform generator.

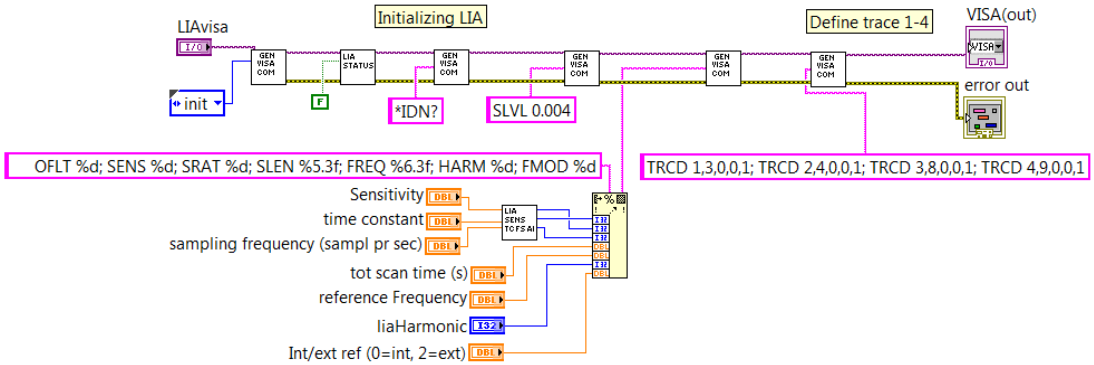

Figure 3.10: Initialising the LIA.

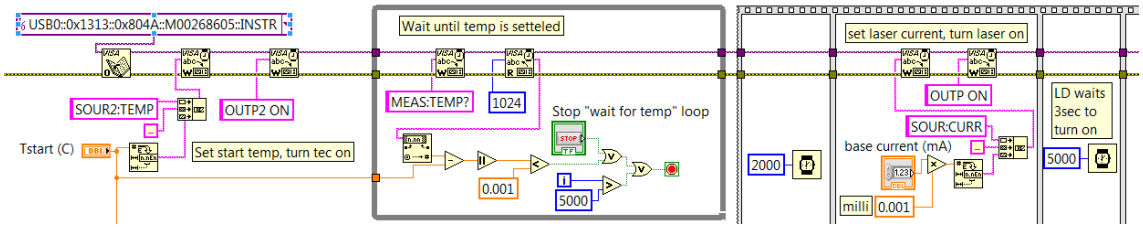

Figure 3.11: Initialising the LD/TC controller

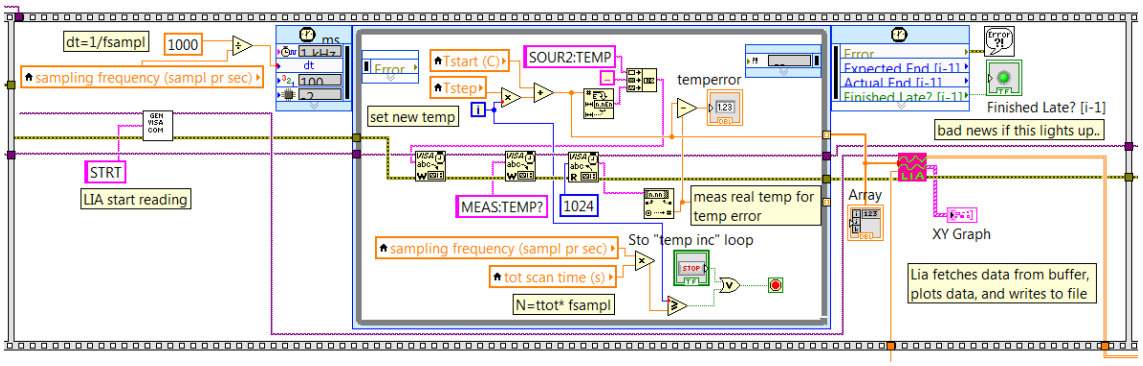

Figure 3.12: Main section of VI where temperature sweep is performed and LIA data is read.

temperature sweep and for the LIA to start reading data. In figure 3.12, this section of the program is shown. Immediately after the LIA is set to start reading data, a timed loop is entered. The temperature is set to increase so that the desired temperature range will be swept during the selected time. For each increase in temperature, the LIA stores one data sample. The difference between the set and the actual temperature is monitored to ensure that the TC can keep up with the desired temperature changes. If it doesn't, the temperature range must be decreased or the total scan time must be increased. The period of the timed loop must be sufficiently long for the commands in the loop to have time to execute. This means that the sampling frequency can not be too high. In the LIA function on the right, the data recorded by the LIA is placed into the LIA buffer and read by the PC. The data is also stored in a 2D array and presented in a XY graph.
When the program terminates, the laser is turned off, and subsequently the TC is turned off and the communication is closed. The data is finally written to file.

In addition to the parts mentioned above, the VI also includes a conversion procedure from temperature to wavelength based on the data given in the data sheet of the laser. In order to calculate the laser wavelength, the

temperature and current must be known. During amplitude modulation, the current is simply the maximum current when the laser is on. During phase modulation, the current is the base current without the added modulation amplitude, since the modulation amplitude oscillates around zero. A LabVIEW case structure is added to determine which modulation is used. The current and the temperature array is input into a Mathscript procedure. The wavelength is 2002.000 nm at 40^o C and 40 mA. It changes 0.046 nm/mA and 0.160 $nm/^oC$. higher than these conditions. Equation 3.4 show how the wavelength is calculated.

$$\lambda = 2002.000 + (I - 40) * 0.046 + (T - 40) * 0.160 \tag{3.4}$$

I is given in mA and T is given in ^oC. λ is given in nm. Figure 3.13 shows a plot of this equation for a range of currents and temperatures.

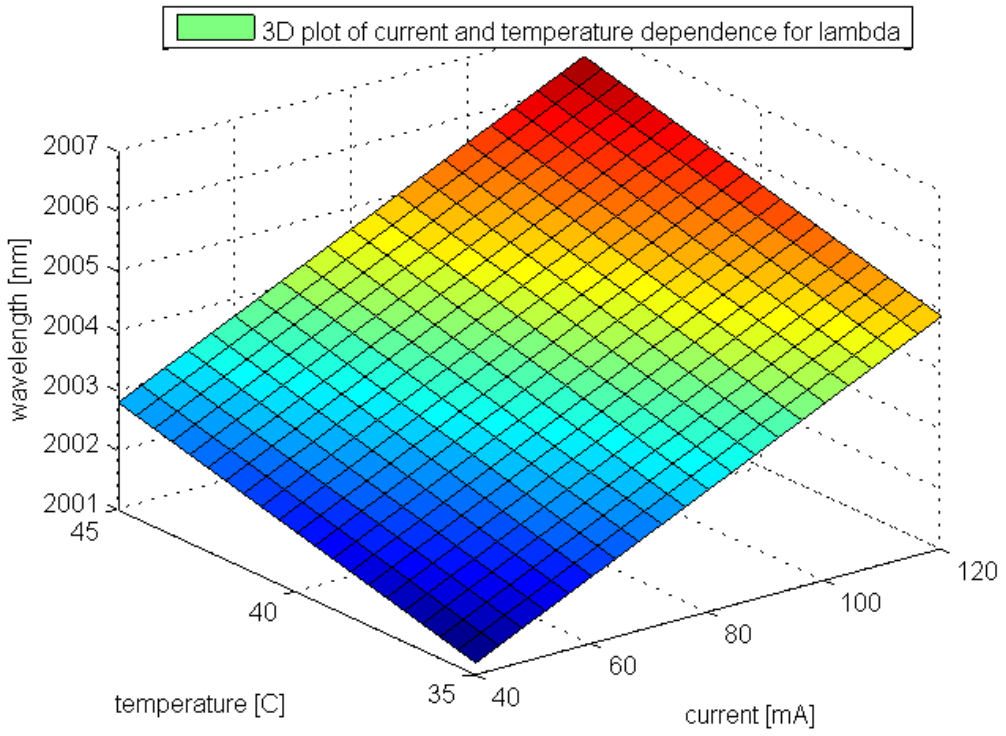

Figure 3.13: Wavelength variations with temperature and current.

Results

The developed LabVIEW VI is quite simple. An improvement for further studies could be to include the ability to turn on and change the variables of the measurement devices without having to redo the entire temperature sweep. The program also needs an improved way to be able to abort midway through its execution. Options should be added to be able to perform multiple sweeps without terminating the program. Certain variables that has been set manually, like the current limit, can be added into the program. The advantage is more user options, the disadvantage is a more complicated and less user-friendly program. For the simple spectroscopy measurements taken in this project, writing a more advanced code takes more time than the effort worth concerning its outcome..

3.2.4 Characterising the laser diode

Motivation

In the operating range of the laser diode, the power is more or less proportional to the current being sent through the LD. At low currents, the current is not high enough for stimulated emission to dominate. Hence, spontaneous emission dominates, and the LD behaves like a LED. In the data-sheet, the threshold current of the nanoplus laser which is where stimulated emission starts dominating, is 11 mA. This value is an estimate for the threshold current for this specific laser model. Variations may occur for individual lasers of the same model. This is why the laser characteristics will be investigated in this section. It is useful to be aware of the variation of power with regard to input current in case it impacts the results of the experiments.

Execution

LabVIEW was used to control Thorlab ITC4005 laser driver and Thorlab PM100D power meter. The laser temperature was $T = 35^o$ and the current was scanned from 0 to 109 mA. For every current value, the power of the laser light at the rear of the PA cell was measured.

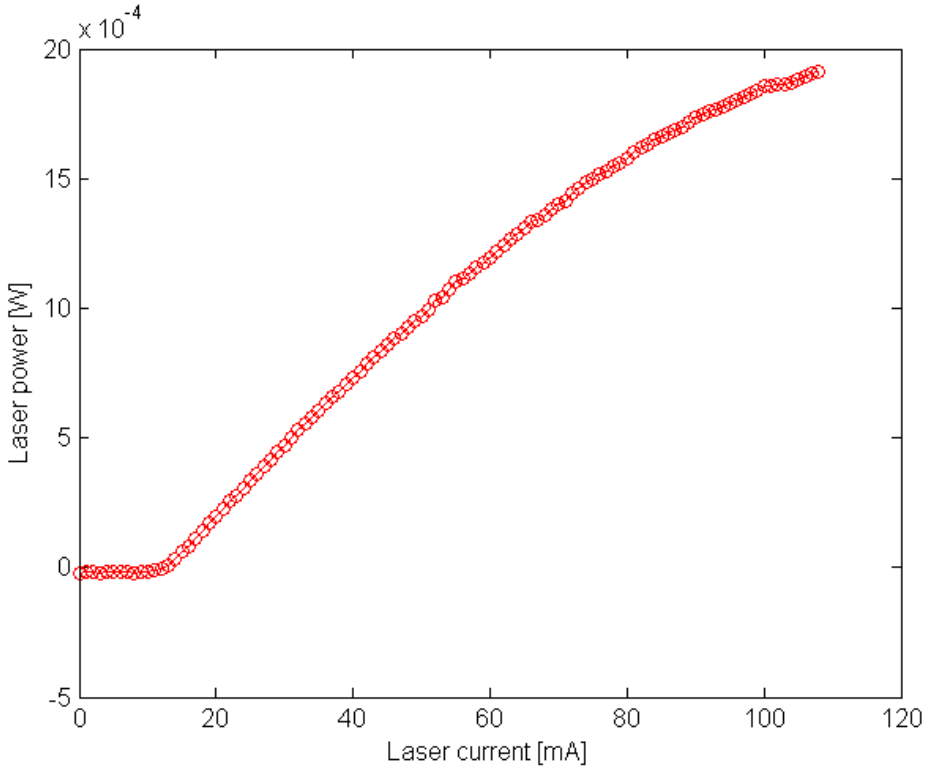

Figure 3.14: Laser diode characteristics. Threshold current of the nanoplus laser diode is approximately 12 mA.

Results

Figure 3.14 show the measured LD . The threshold current is 12 mA which is very close to what was expected. Also notice that the power curve flattens out for higher currents.

3.2.5 The effect of water

Motivation

In using flow controllers to mix CO_2 and N_2, the goal is to control the CO_2 concentration. Regular air does however contain water vapour and Argon. Water has an absorption band at approximately 2004.5 nm, which is in the range of the laser. It is therefore necessary to investigate how water vapour affect the PA signal.
The presence of Argon will also affect the PA signal. A resonant energy transfer between the excited state of CO_2 and the nearby vibration level of N_2 results in a slow thermalisation of the light energy, thus reducing the efficiency of the PA signal generation. Adding Argon will decrease this effect, resulting in an increase in the PA signal (Gebhardt and Smith, 1972). The PA signal for CO_2 in pure Argon is about 2.5 times larger than the PA signal for CO_2 in pure N_2. With the atmosphere containing less than 1% Argon, the absence of Argon in the $CO_2 - N_2$ gas mix should not influence significantly, but is worth being mentioned. The effect of varying Argon concentrations is not investigated in this project. The PA signal emerging from air will be compared to that of the $CO_2 - N_2$ gas mix.

Execution

Two experiments are performed. First approximately 3 ml of water is placed in one of the buffers. The measurement cell is then filled with 400 ppm of CO_2 gas. A PA measurement is made once every 5 minute to see what happens to the PA signal as the water vaporises. Secondly, a PA measurement is made where the measurement cell is filled with pure N_2 with water still present in the buffer. This signal is added to the PA signal obtained for 400 ppm of CO_2 gas with no water, and compared to the PA signal of natural air. The second experiment demonstrates that PA signals can be added to study the PA signal of a mixed gases. The PA signal for pure N_2 was also measured to determine the noise level, and to ensure that no unexpected signals were picked up.

Results

Figure 3.15 show how the PA signal at 2004.9 nm increases as more water vaporises, while the other peaks remain relatively the same. From figure 3.3 we expect the water absorption line to be at 2004.6 nm. This slight shift in wavelength can be attributed to a number of things. The constants used to calculate the wavelength is taken from the data sheet. There is a possibility that the constants are not calibrated for this specific laser, and thereby causing the deviation. Another possibility is that the PA signal peak may shift. It can be seen from figure 3.15 that the peak does shift somewhat with increasing vapour.

Figure 3.16 shows that adding the PA signal obtained for 400 ppm CO_2 with the PA signal obtained for N_2 with water vapour is similar to the PA signal of air consisting of 400 ppm CO_2 and water vapour. The PA signal with only water vapour is taken after 10 minutes, where the water has had time to vaporise. For the other peaks, which should be unaffected by the water vapour, the PA signal is somewhat lower than the signal emerging from air. In addition to the effect of Argon, the PA signal could be lower due to the mixing of CO_2 and N_2 which had not been calibrated. This is discussed further in section 3.2.7.

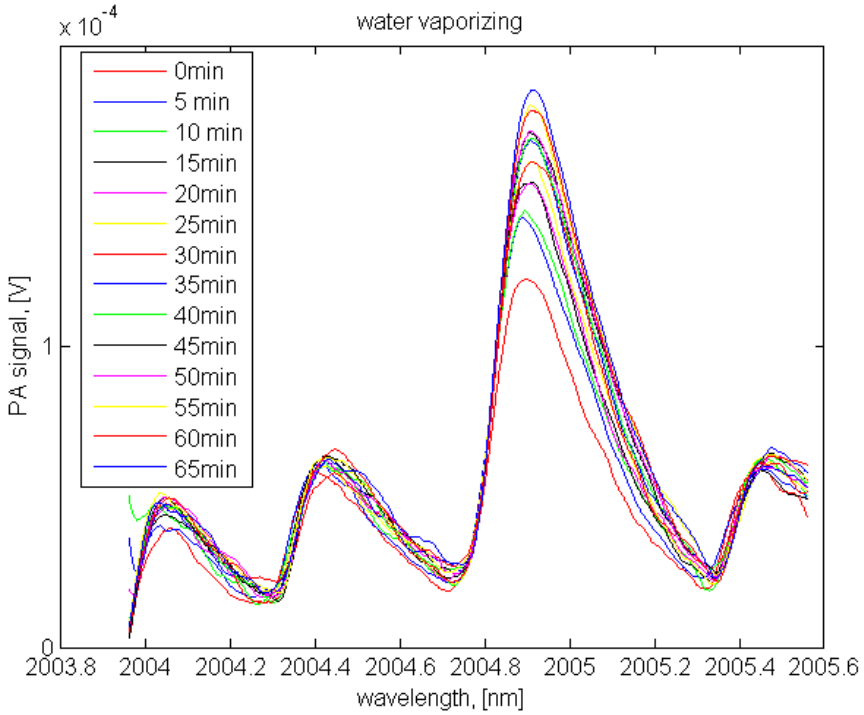

Figure 3.15: Water vaporising affecting the PA signal.

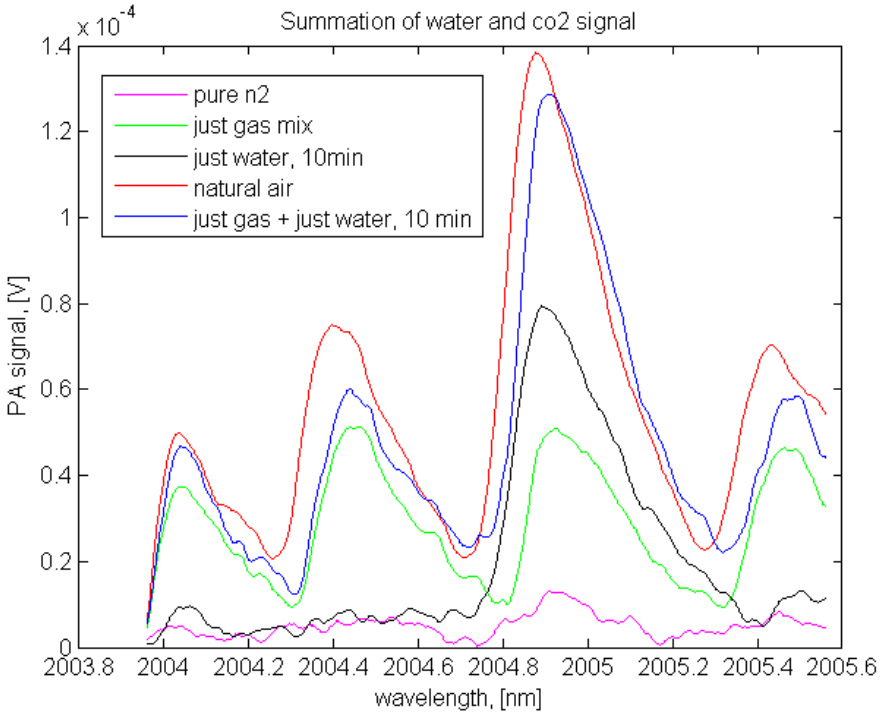

Figure 3.16: Adding the CO_2 signal with the H_2O signal.

3.2.6 Linearity of PA signal with regard to concentration

Motivation

One of the more fascinating issues concerning PAS is the range over which it works. The PA response is linear over several decades. In fact, the gradient should be the same for all concentrations. The sensitivity settings from the LIA causes however the offset to be different for different sensitivities.
The resonance frequency of the measurement cell was found using a speaker, not a PA signal, and was measured in air. As explained earlier, the resonance frequency is dependent on the speed of sound of the medium inside the cell. The speed of sound in air is approximately 343 m/s. The speed of sound in N_2 is 353 m/s and for pure CO_2 it is 270 m/s. In other words, the speed of sound is dependent on the components, and subsequently the resonance frequency. The resonance frequency is proportional to the speed of sound, see equation 3.3. Since the speed of sound is lower for CO_2 than N_2, the resonance frequency is expected to decrease with increasing CO_2 concentrations. The resonance frequency will therefore be re-validated using PA for various gas mixtures.
By knowing the concentration of the gas, and finding the gradient and offset, the goal is to calibrate the detector.

Execution

The flow-controllers are used to mix CO_2 and N_2. The controller for the N_2 gas has a maximum flow of 5 ln/min at 2 atm input pressure and 20^o C. ln/min means l/min at normal conditions i.e. 0^o C and 1 atm. The controller for the CO_2 gas has a flow of 10 mln/min under the same conditions. The regulators on the gas tanks are therefore set to 2 atm. The room temperature is approximately 22^o C, and no corrections are made to compensate for this temperature difference. The effect of this and other measurement uncertainties will be discussed in the next section. The CO_2 concentration

a_{CO_2} is calculated using the equation:

$$a_{CO_2} = \frac{0.01 p_{CO_2}}{0.01 p_{CO_2} + 5 p_{N_2}} \tag{3.5}$$

where p_{CO_2} is the percentage opening of the CO_2 flow controller valve, and p_{N_2} is the percentage opening of the N_2 controller valve. The gas is left flowing for a few minutes for the PID controller of the flow controllers to stabilise and for the measurement cell to be properly purged. The valve opening is checked to have the correct value.
After the measurement cell has been filled with gas, six consecutive modulation frequency sweeps are done for some of the mixtures. For each sweep, a Gaussian curve with a peak at the resonance frequency is obtained. The mean and standard deviation of the six measurements is calculated. As will be discussed in the next section, the measurement uncertainty of the PA measurement is difficult to quantify exactly since there are many unknown factors present. Instead, repeatability measurements are used to determine the accuracy of the measurement. Six PA sweeps are also conducted using the measured modulation frequency. The mean and standard deviation is calculated, and the maximum value of the 2004.5 nm peak, which is the peak unaffected by water vapour, is plotted against the CO_2 concentration. All the measurements are conducted with the LIA time constant set to 3 s, a sampling rate of 8 $samples/s$ and a scan time of 200 s. The laser is amplitude modulated using $10 - 100$ mA current. Linear regression is used to determine the gradient of the response. A distinction between measurements with different sensitivities is made, and the gradients compared. A single PA signal was also measured for concentrations between 2 and 10% CO_2 using a modulation frequency of 1310 Hz.

Results

The concentrations and sensitivities used are presented in table 3.1. From the table it can be seen that the resonance frequency is not as measured earlier, but does not vary significantly in the range it has been measured. As expected it is slightly lower for the highest concentration for which it has been measured, but the variation is not significant for the PA signal for the lower

p_{N2}, [%]	p_{CO2}, [%]	a_c, [ppm]	sensitivity [V/A]	Res. freq. [Hz]	Q-factor
100	10	200	100e-6	1330 ± 4	19.28
90	10	222	100e-6	1337 ± 5	16.92
80	10	250	100e-6		
70	10	286	100e-6		
60	10	333	100e-6		
50	10	400	100e-6		
50	10	400	500e-6	1329 ± 6	17.26
50	20	799	500e-6	1333 ± 2	18.02
50	30	1199	500e-6	1333 ± 3	18.01
50	40	1597	500e-6	1332 ± 2	18.24
50	50	1996	500e-6	1332 ± 2	18.24
50	60	2394	500e-6	1333 ± 2	18.26
50	70	2792	500e-6	1332 ± 4	18.00
50	80	3190	500e-6	1334 ± 2	N.A
50	90	3587	500e-6	1333 ± 1	N.A
50	100	3984	500e-6	1333 ± 1	N.A
50	100	3984	5e-3		
40	100	4975	5e-3		
30	100	6623	5e-3		
20	100	9901	5e-3		
10	80	15748	5e-3		
10	100	19608	5e-3	1327 ± 1	N.A
9.70	100	20000	100e-3		
4.75	100	40000	100e-3		
3.10	100	60000	100e-3		
2.28	100	70000	100e-3		
1.78	100	100000	100e-3		

Table 3.1: The concentrations and sensitivities that are used, and the result for the frequency sweep.

concentrations. The concentrations between $2 - 10\%$ were all taken at 1310 Hz. The variation in resonance frequency may be larger for these data point, as the range is larger. For more accurate results, the resonance frequency should be measured, and multiple PA signals should be measured for each sample. However, the large concentrations are meant only to demonstrate the coincidence of the gradient also at higher concentrations, and time is not spent on achieving higher accuracy.

Figure 3.17 shows the data acquired for concentrations measured with a sensitivity of $500e - 6\ V$. The maximum value of the 2004.5 nm peak is plotted in figure 3.18, along with the standard deviation at this point. A

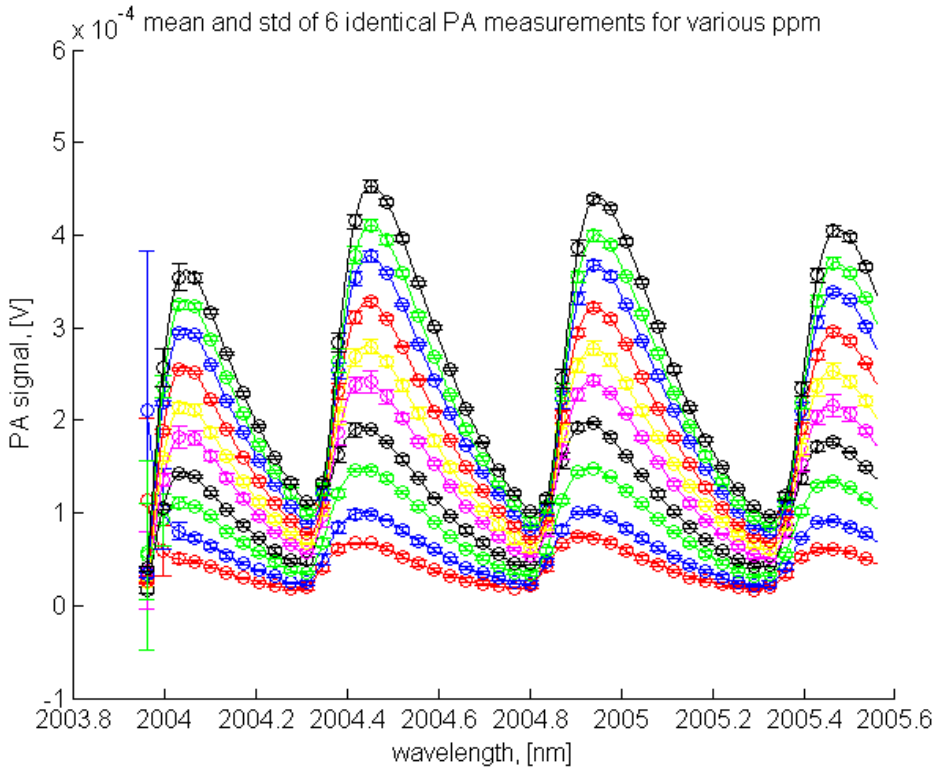

Figure 3.17: PA signal mean and standard deviation for concentration measured with a sensitivity of $500e-6\ V$.

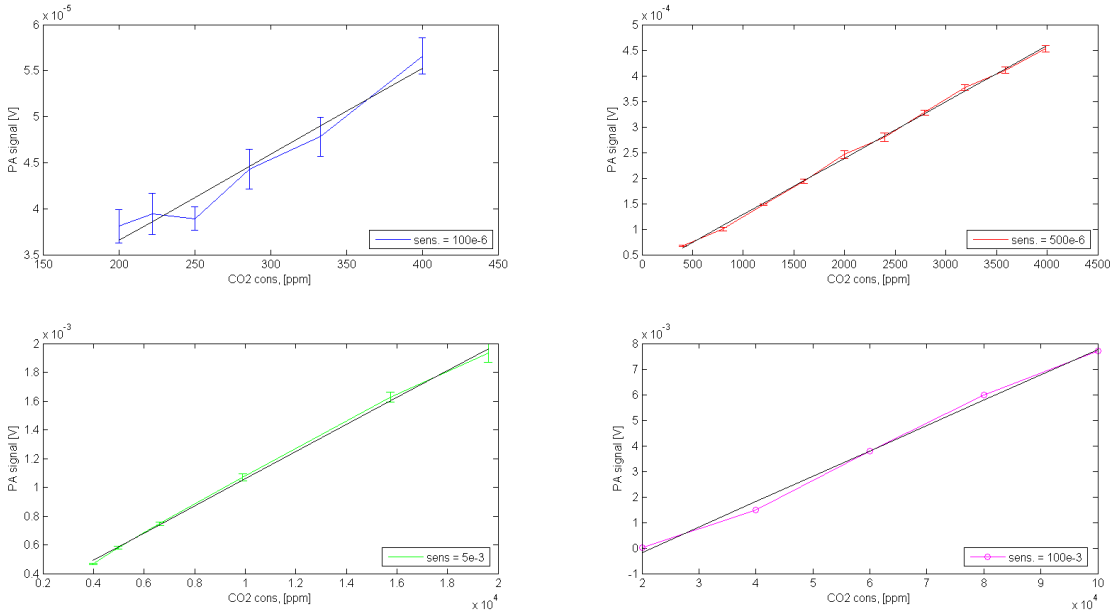

Figure 3.18: Maximum value of 2004.5 nm peak for various concentrations.

plot is made for each of the other sensitivities as well. Along with the data, a linear regression line is also plotted, and the gradient, offset and regression value is presented in table 3.2. As expected, the offset varies due to the change in sensitivity. The gradient is remarkably similar, especially for the $200 - 400$ *ppm* and $3948 - 19608$ *ppm* samples. The $200 - 400$ *ppm* data points are less linear probably because this is closer to the noise level, and the low flow in the flow controllers leads to less accurate concentration of the mixed gas.
The goal, to calibrate the detector has been achieved. The gradient has been found, and is quite consistent over a large range. The offset must be chosen according to the sensitivity setting.

3.2.7 Measurement uncertainty

To find the measurement uncertainty of a system, the uncertainty of each element in the system must be known, and a model of how the different components affect each other, including the conversion factors or sensitivities, must also be known. The combined standard uncertainty for adding and subtracting measurement uncertainties is

$$u = \sqrt{u_1^2 + u_2^2 + ... + u_i} \tag{3.6}$$

where u is the combined measurement uncertainty and u_i is the uncertainty of the included elements. For multiplication or division the combined relative uncertainty is

$$\frac{u(A)}{A} = \sqrt{\frac{u(B)^2}{B^2} + \frac{u(C)^2}{C^2} + ...} \tag{3.7}$$

where u(A) is the uncertainty of the value A composed of values B, C and so on, each with measurement uncertainty u(B), u(C).

Gas mixture

From the data sheet of the gas controllers, the uncertainty is found to be $\frac{u(valve)}{valve} = 0.4\%$ for both controllers. The CO_2 concentration is determined using equation 3.5, and the measurement uncertainty for a_{CO2} is then calcu-

concentration range, [ppm]	gradient	offset	regression value
200-400	93.249e-9	1.7919e-5	0.9769
400-3984	109.94e-9	1.9273e-5	0.9993
3984 - 19608	94.298e-9	1.1529e-4	0.9992
20000 - 100000	99.386e-9	-0.0022	0.9977

Table 3.2: The gradient, offset and regression value of the four slopes shown in figure 3.18

lated as

$$\frac{u(a_{CO2})}{a_{CO2}} = \sqrt{\frac{u(valve)^2}{valve^2} + \frac{(\frac{u(valve)}{valve}0.01p_{co2})^2 + (\frac{u(valve)}{valve}5p_{n2})^2}{(0.01p_{co2} + 5p_{n2})^2}} = 0.57\% \tag{3.8}$$

Variations in pressure and temperature will affect the flow through the flow controllers, however the rates for these changes are not given in the data sheet, and the pressure and temperature is kept constant.
The tubes connecting the two controllers were checked for leakages. A small leakage may cause large changes in CO_2 concentration. The leakage check is done by closing the exit tube and opening the flow valves to increase the pressure in the tubes. The N_2 valve is then closed and the flow is measured using the CO_2 controller, seeing as it is the more sensitive controller. The measured flow was 0 mln/min, so the tubes can be assumed not to leak. The high linearity in the PA signal indicates that the flow controllers does not have any non-linear errors.

The PA signal

Unfortunately there is no detailed model of the PA process for the experimental setup that has been developed. The measurement uncertainty in the laser power caused by the measurement uncertainty in the external modulation and the LDD, can be calculated. The measurement uncertainty in the microphone signal and its effect on the LIA output uncertainty can also be calculated. However, how much of the light is dissipated in the fibre and reflected off the glass, is not known. The laser light power can be measured in the measurement cell, and the measurement uncertainty of the power meter can be used instead of the measurement uncertainty of the laser output. Even so, the exact light absorption conversion factors are unknown, and how

much is transformed into heat, and what pressure it causes. Table 3.3 lists the known measurement uncertainty factors. The most significant contributor to the measurement uncertainty of the outgoing laser power is the modifying and interfering uncertainty of Agilent 33500B function generator, and the interfering uncertainty of Thorlabs ITC4005 laser current.

Since it is difficult to quantify the measurement uncertainty based on the known accuracy of the instruments, the statistical representation of the measurement elements are considered. From the standard deviation of the measurements, the accuracy has been calculated for the lower, medium and higher concentration range and can be found in table 3.4. The minimum standard deviation $\sigma_{PA}(min)$ and the maximum standard deviation $\sigma_{PA}(max)$ for the respective measurement ranges are listed. The mean accuracy has also been calculated using $mean\ accuracy = \sigma_{PA}/PA\ signal$. The lower range has the highest uncertainty. An improved measurement uncertainty may have been achieved using more PA samples. Also, by using the internal modulator in Thorlab ITC4005 the uncertainty introduced by the Agilent 33500B signal generator would have been eliminated. External factors like acoustic noise emerging from the building have increased the noise picked up by the microphone, and that has probably affected the lower PA signals more, making them the most inaccurate.

The exact value of the detection limit could not be found because the gas flow controllers can not mix the gas accurately in such small concentrations. However, PA signals can be distinguished from noise at least down to approximately 20 μV. Using the regression values from table 3.2 this corresponds to a concentration of 20 ppm.

Device	modifying u	interfering u
Agilent 33500B waveform generator amplitude	1%	$\pm 1\ mV_{pp}$
Agilent 33500B waveform generator frequency	1%	$\pm 15\ pHz$
Thorlabs ITC4005 LDD/TC laser current	0.1%	$\pm 2\ mA$
Thorlabs ITC4005 LDD/TC TEC current controll	0.2%	$\pm 20\ mA$
Sennheiser KE 4-211-2 Microphone	$\pm 2.5\ dB$	
Standford Research system SR850 LIA	$\pm 1\%$	

Table 3.3: Measurement uncertainties of the various components in the PA setup. An interfering input causes a constant deviation from the desired value, whereas a modifying input is a systematic error, where the size of the error depends on some variable.

ppm values	$\sigma_{PA}(min)$ [V]	$\sigma_{PA}(max)$ [V]	mean accuracy [%]
200-400	0.1254e-5	0.2258e-5	4.42
400-3984	0.0942e-5	0.8056e-5	2.01
3984-19608	0.418e-5	6.539e-5	2.02

Table 3.4: Measurement uncertainty based on repeatability

Chapter 4

CO_2 in water

4.1 Models and methods

The properties of light and acoustic signal in water are quite different from those in air. From the optical point of view, the dependence of the shape of the acoustic wave to the absorption has already been investigated. Looking at the acoustic properties, the acoustic impedance is different, possibly causing the acoustic signal to attenuate and reflect differently. First, reflectance is investigated, then secondly, attenuation will be investigated.
The reflection and transmission coefficients R and T for sound waves are expressed in terms of the acoustic impedances Z_1 and Z_2 of the materials forming the interface.

$$R = (\frac{Z_2 - Z_1}{Z_2 + Z_1})^2 \tag{4.1}$$

$$T = 1 - (\frac{Z_2 - Z_1}{Z_2 + Z_1})^2 \tag{4.2}$$

The characteristic impedance is $Z = \rho c$ where ρ is the density and c is the speed of sound for the medium in question (NDT Resource centre). Using equation 4.1 and 4.2 and the values given in table **??**, it can be shown that an acoustic wave travelling in water inside stainless steel measurement cell will reflect 88% and transmit 12% of its signal. The transmitted sound travelling in the steel will be reflected at the steel-air boundary. An issue occurring when sound is reflected is that it may change the phase of the signal. When arriving at the transducer it may be out of phase with other parts of the

Medium	ρ $[kg/m^3]$	c $[m/s]$	Z $[Rayl]$
Water	997.8	1497	1.48 M
Stainless steel	7890	5790	45.16 M
Air	1.2	343	413

Table 4.1: The density, speed of sound and acoustic impedance are given for water, stainless steel and air (NDT Resource centre), (Cobbold, 2007).

signal.

The attenuation of sound in water depends on a number of factors, e.g. frequency, temperature, depth, salinity and even acidity. Ainslie & McColm's article from 1998 presents a simplified equation for calculating the attenuation coefficient in water:

$$\alpha = 0.106\frac{f_1 f^2}{f^2+f_1^2}e^{(pH-8)/0.56}+0.52(1+\frac{T}{43})(\frac{S}{35})\frac{f_2 f^2}{f^2+f_2^2}e^{-z/6}+0.00049f^2e^{-(T/27+z/17)} \tag{4.3}$$

where the temperature is $-6^o\ C < T < 35^o\ C$, the acidity value is $7.7 < pH < 8.3$, the salinity is $5\ ppt < S < 50\ ppt$, and the depth is $0 < z < 7\ km$. $f_1 = 0.78(S/35)^{0.5}e^{(T/26)}$ and $f_2 = 42e^{(T/17)}$. This equation shows that the absorption is higher for higher frequencies.

An attempt was made to determine the expected amplitude of the acoustic signal generated from the laser beam. A number of assumptions was made which are most likely incorrect, but will help in determining the maximum achievable PA signal. The first assumption is that the entire optical power from the laser is converted to acoustic power. This power can be expressed as

$$P = pvA \tag{4.4}$$

p is the acoustic pressure, v is the particle velocity and A is the area over which the sound wave has propagated, $A = 4\pi r^2$, r is the distance the acoustic wave has travelled from the source of the PA signal to the transducer. The particle velocity can be expressed using the acoustic pressure and impedance, $v = p/Z$. Solving for p, and multiplying with the gain coefficient G of the transducer in use gives the voltage amplitude of the acoustic signal.

$$V = G\sqrt{\frac{PZ}{4\pi r^2}} \tag{4.5}$$

The specific impedance $Z = p/v = R + iX$ is equal to the characteristic acoustic impedance $Z_{char} = c\rho$ for planar single frequency waves. Viscous medium causes a phase difference between the pressure and particle velocity making Z complex, and containing phasors which depend on the position and frequency. Water is not particularly viscous, so for calculating the maximum achievable signal, the specific impedance is used. However, keep in mind that the acoustic signal may be position and frequency dependent. The following values are needed to solve eq. 4.5: $P = 1\ mW$, which is measured with the power meter. It may not be very accurate as the light travels differently through glass into water, than through glass into air. The figures for c and ρ have already been given. The measurement cell has been designed so that $r = 3.5\ cm$. $G = 25.3\ \mu V/Pa$. This gives $p_{max} = 312\ Pa$ and $V_{max} = 7.9\ mV$. Only a part of the signal will travel directly to the transducer. The remaining parts will reflect off the walls of the measurement cell. This is only a theoretical value, and has not been measured.

4.2 Experiments

4.2.1 Investigating frequencies and wavelengths in search of a signal

Motivation

Before any CO_2 concentration analysis in water can be made, it must be determined whether a PA signal actually can be obtained. Investigations are made to find the most suited excitation frequency, and at which wavelengths the absorption peaks occur.

Execution

Using the 6 cm measurement cell, frequency sweeps was done at $T = 38^o$ C, first for a low frequency range, and subsequently for the entire frequency range. The ITC4005 LDD/TC has a maximum modulation frequency for the internal modulator of 100 kHz. The Agilent function generator and the LIA also have a maximum frequency of 100 kHz. The maximum frequency for the hydrophone is higher than this, and this is therefore considered the modulation limit for the system. For the lower frequency range, scans were performed where the laser was turned off, so the signal with the laser on could be compared to the noise level. Also, a PA signal was measured over the upper half of the wavelength range for a low, medium and high frequency. The experimental setup illustrated in figure 4.1 is used.

Results

In figure 4.2 it can be seen that the signal consists of noise only, both when the laser is on and when it is off. The black and blue lines show the signal measured between $0 - 200$ Hz. The reason the red and pink graph show a lower signal is because they are measured with a higher time constant. It is also relevant to note that the noise level is much higher at low frequencies. Higher signals at low frequencies must not be mistaken for PA signals. Only noise level signals are detected in the scan spanning the entire frequency

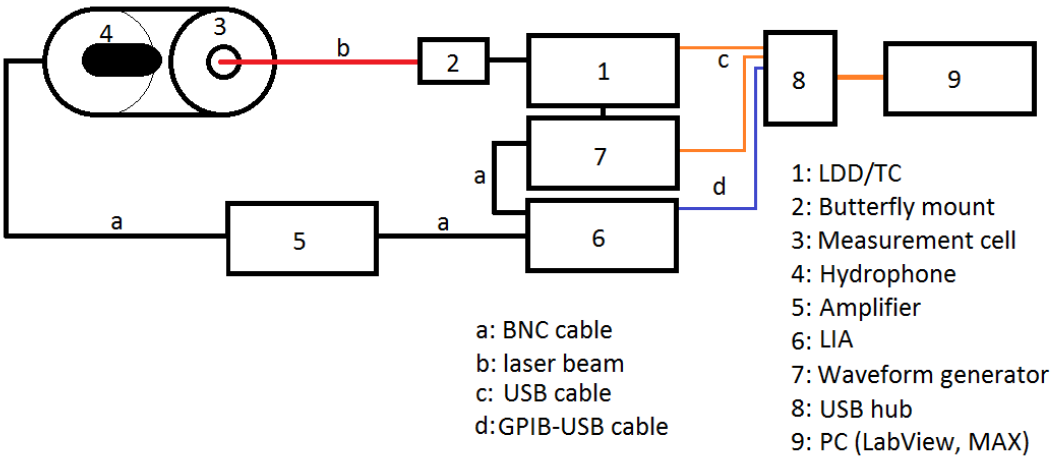

Figure 4.1: Initial experimental set-up for experiments in water.

range, and the scan shows that the noise level is lower for higher frequencies. The wavelength scans shows that all the signals are as low as the noise level for the respective frequencies, and show no PA absorption peaks.
based on the above, either a PA signal is not being generated, or it is not being detected.

4.2.2 Trouble shooting

Motivation

An explanation for why a PA signal could not be found must be given. It could be a number of reasons, some are rectifiable, whereas others are not. In the following, a number of reasons are presented along with a suggestion of how to deal with the challenge.

Execution

- Absorption lines in the given wavelength region.
  Figure 4.3 shows the electromagnetic absorption coefficient for water. At 2000 nm, $\alpha_{water} \approx 70\ cm^{-1}$, (Wieliczka et al., 1989). This is much higher than the absorption coefficient for water vapour of approximately $1.2 * 10^{-4}\ cm^{-1}$, see figure 3.3. The penetration depth is

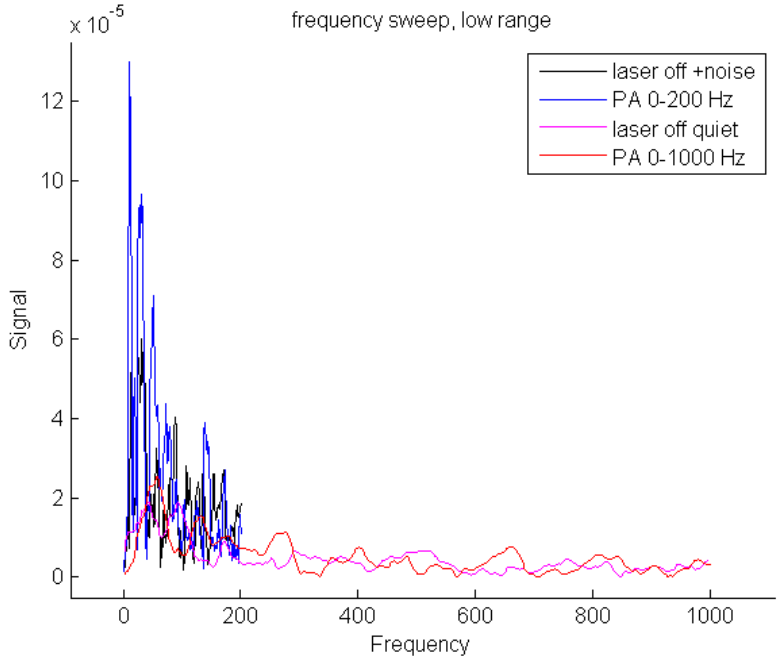

Figure 4.2: Frequency scan done with $T = 38^o\ C$ with and without the laser turned on to determine if PA signal is achieved and to investigate noise level.

given by $\delta = 1/\alpha = 0.14\ mm$. Most of the light will be absorbed immediately within the measurement cell. This means that, regardless of the CO_2 content, a PA signal should be obtained by the water that is present.

No data could be found in existing literature about the absorption coefficient of CO_2 or H_2CO_3 in water. It is not given that it is the same as the absorption coefficient for CO_2 in gas. If a PA signal from water is achieved, it will reveal the absorption spectra fo CO_2 in water. To conclude, there is no explanation for why a PA signal is not generated in regards to the absorption coefficients, because water has such a high absorption coefficient.

- Collimation.

  The laser is collimated as well as possible given the available opto-mechanical equipment. Unfortunately, only a $600 - 1050\ nm$ coated collimation lens was available and it stops part of the light. A power meter is used to control the collimation of the laser, since the beam cannot be seen with the naked eye. After the beam has been properly collimated, the power is measured to be between $1 - 1.5\ mW$. Even

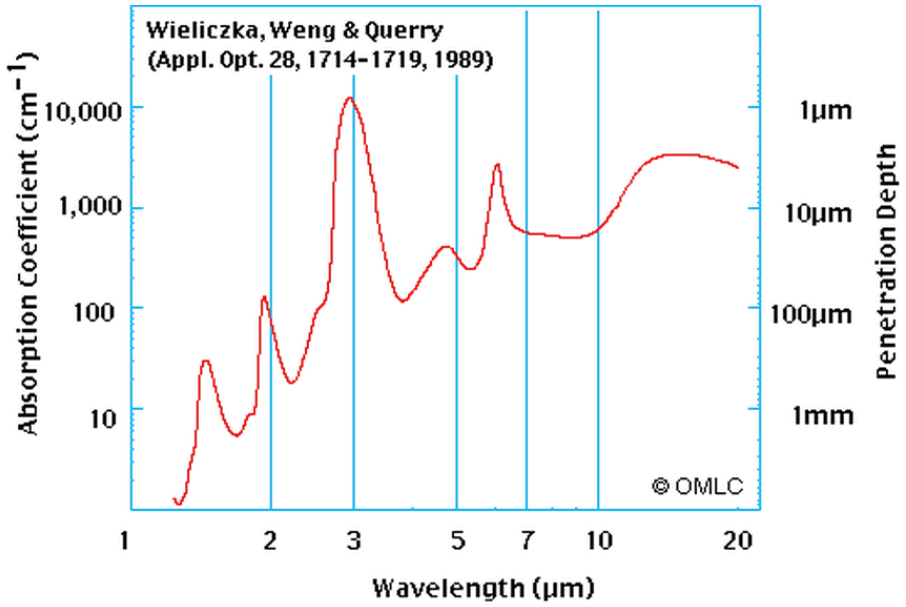

Figure 4.3: Absorption coefficient of water, (Wieliczka et al., 1989)

when collimated the beam width is about the same as the width of the window. As a consequence, the shape of the generated sound wave will be equivalent to a wave made by a piston source. This is not necessarily negative, as that wave will be plane at a shorter distance, but PA signals generated in this fashion is not mentioned in literature. The reason for this is most likely that such a wide beam causes the intensity of the beam at one point to be much lower. The power of the laser is already very low compared to what is used in similar projects. This problem can be addressed by acquiring a NIR-coated lens, appropriate for this given wavelength, and place it to create a focal point immediately inside the cell window.

- Relaxation time.
  If the relaxation time is longer than the pulse frequency, the molecules will not have time to free the absorbed energy before absorbing more energy. The relaxation time varies for different molecules and for different solvents. The relaxation time for vibrational energy in water is in the order of ns (Deàk et al., 2000). The frequency range of the laser is up to 100 kHz, which leaves plenty of time for relaxation. A modulation frequency in the MHz region would be at the limit of the time needed for relaxation. The restraint the relaxation time puts on

the modulation frequency is therefore something one should be aware of, but is not a problem in this project.

- Laser power
  Pulsed lasers are more common to use in PAS than continuous power lasers. Pulsed lasers give a much more concentrated energy pulse. Even though a PA signal was achieved in gas, the laser might be too weak to make an effect in water. In gas, the PA signal generation is based on the expansion of a gas. Because the expansion coefficient in water is so much smaller, a strong detectable signal could be generated by vaporisation and boiling which causes shock waves. For that to occur, the laser energy within the absorbing region must be above a given threshold. For water this threshold is 2.24 kJ/cm^3 (Zhao and Zuomin, 2002). Given the penetration depth and window size of the cell, the volume the light is deposited in is $V = \delta\pi r^2 = 0.0099\ cm^3$. The laser must have a minimum energy of $E = 22.2\ J$ to generate boiling. The nanoplus laser is not powerful enough to cause boiling. Replacing the laser with a more powerful, preferably pulsed laser would help. A cheaper solution would be to collimate the beam better, to increase the intensity at a single point.

- Attenuation of sound.
  Sound in water has a frequency between $10\ Hz < f < 1\ MHz$. Absorption of sound for low frequencies is weak. The main reason for attenuation in liquids is viscosity, and losses at boundaries. In addition to attenuating the signal, viscosity causes a phase change in the signal. Water is not particularly viscous, so this is not a significant issue. However changing the length of the measurement cell may change the interference pattern of the sound signal at the hydrophone. The attenuation of sound is calculated to be 0 dB/cm at frequency $f = 30\ Hz$, $5.15 * 10^{-6}\ dB/cm$ at $f = 21\ kHz$, and $64.65 * 10^{-6}\ dB/cm$ at $f = 90\ kHz$. It is calculated for water with 5 *ppt* salinity, $20^o\ C$, at atmospheric pressure (Ainslie & McColm, 1998), (NPL). All in all, a very small attenuation compared to losses at the boundary.
  As mentioned earlier, 88% of the sound is reflected at the boundary. The transmitted sound is later reflected at the steel-air boundary, contributing to the phase distortion of the signal. For good measures sake,

a smaller measurement cell of 3.5 cm was made, in order to get the hydrophone closer to the window where the signal is generated. A pre-amplifier was also used between the hydrophone and the LIA, which boosts the signal of the hydrophone so the combined gain is no longer 23.5 $\mu V/Pa$, but 31.5 mV/Pa.

- Expansion coefficient.
  The model for generating a PA signal given in chapter 2 (Patel and Tam, 1981) describes an adiabatic, isobaric expansion of an ideal gas. Two concerns arise in this regard. Firstly, water is not an ideal gas, and may behave differently. This does not exclude the possibility of generating a PA signal, but a different model must be used. Secondly, the thermal expansion coefficient for water is much smaller than for air: $\beta_{air} = 3430e-6\ K^{-1}$, $\beta_{water} = 207e-6\ K^{-1}$. The acoustic signal generated by thermal expansion in water will therefore be much smaller, possibly too small to be detected. A solution will be to increase the power of the laser to achieve boiling. This was explained under the item "Laser power". But increasing the laser power violates the premises for this thesis, which was to create a cheap low power instrument. Instead of approaching this as a gas sample problem, it should be approached as a solid sample problem. In PAS of solids, the acoustic signal is often detected with a microphone in the gas directly above the sample. This is worth exploring.

Results

After looking at all the possible reasons for why a PA signal is not being generated, the following modifications are suggested: A smaller measurement cell is made. The main reason for no signal is most likely because of the low thermal expansion coefficient. Buying a more powerful pulsed laser would be the best way to ensure a PA signal. However, that is a somewhat expensive solution. Instead, better focusing lenses was acquired. An alternative measurement cell window configuration was made, allowing the microphone used in the gas detection to be mounted next to the window. The PA signal from the water can then be detected via air.

4.2.3 Achieving PA signal

Motivation

As a result of the previous experiment, improvements are made and another attempt is made at detecting a PA signal for CO_2 in water.

Execution

The new and improved setup is shown in figure 4.4. Two IR-coated ($1.8 - 3$ μm) lenses is used to focus the laser beam at the water surface. The detected laser power is 2.8 mW with this configuration. A thin layer of N_2 gas is added above the water so the microphone can be used to detect the signal from the CO_2 in the water. Soda water which has a CO_2 concentration of $1 - 2\%$ was used initially. Next, fresh rainwater was used.
A frequency scan was initially performed to determine which modulation frequency yields the strongest PA signal.

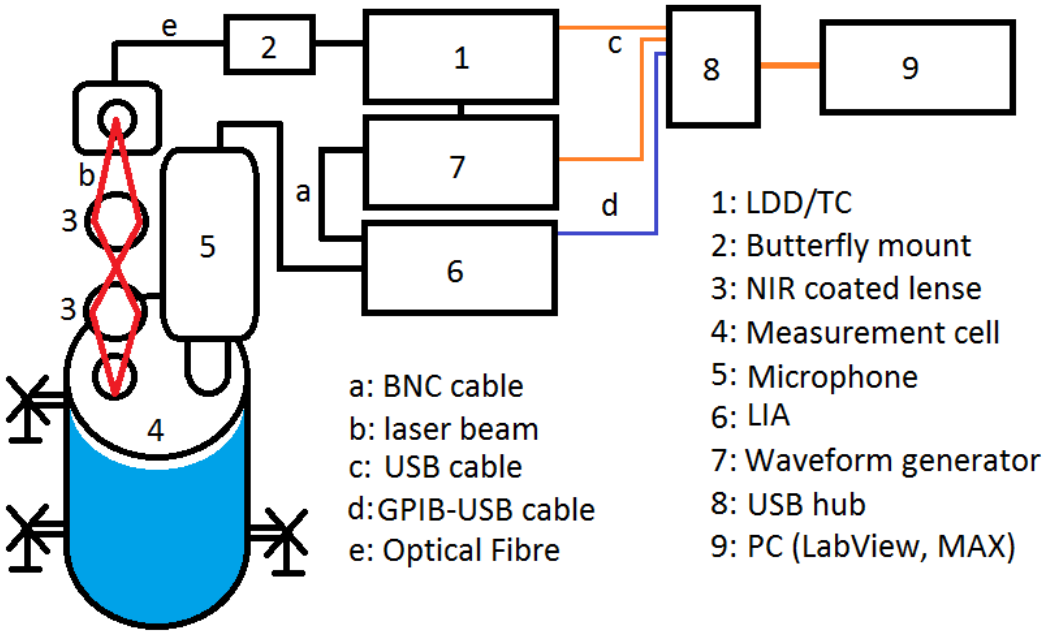

Figure 4.4: Improved experiment set-up for measurements in water

Results

The resulting PA signal is presented in figure 4.5. The signal is strong at first, but then decrease linearly. Later, the signal seems to have reached a steady state value.

Soda water contains more CO_2 than water can contain at atmospheric pressure. When the bottle is opened this results in CO_2 gas bubbling from the water. When this also happens in the measurement cell, the gas above the water sample will no longer be pure N_2. The PA signal measured is dominantly from the gas layer above the water. The CO_2 that is being detected is from the water sample, but the detection occurs in the gas. As time passes, some of the CO_2 is absorbed back into the water until equilibrium is reached, according to Henry's law

$$p = k_H c$$

where p is partial pressure, k_H is 29.41 $L\Delta atm/mol$ for CO_2, and c is the concentration of the solute. Although the CO_2 concentration can be calculated from the amplitude of the PA signal from the gas above the water and using Henry's law, reaching equilibrium takes several hours, which is not the fast and easy detection in water that was the goal of the project.

For the fresh rainwater, only noise signals were detected both immediately after closing the measurement cell, and several hours later when equilibrium between the water and the gas is expected. The conclusion is that the PA signal for such low concentrations is too weak compared to the noise level.

The noise level is quite high ($\approx 30\ \mu V$), most likely caused by the large water surface which allows ripples to move across the water. Further work should include designing a smaller measurement cell for measurements in water.

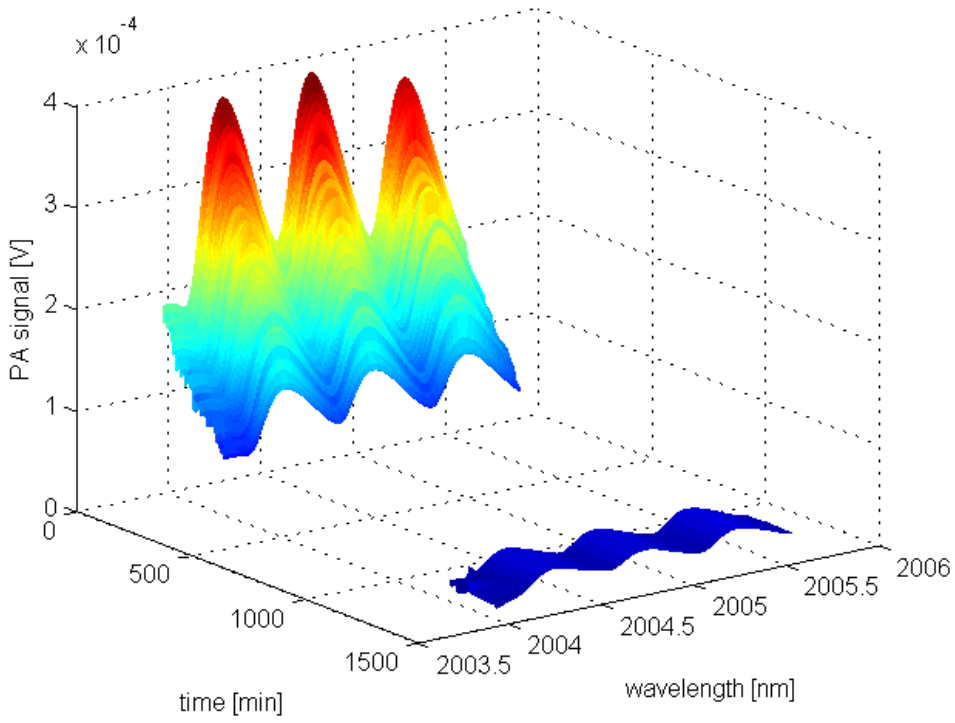

(a)

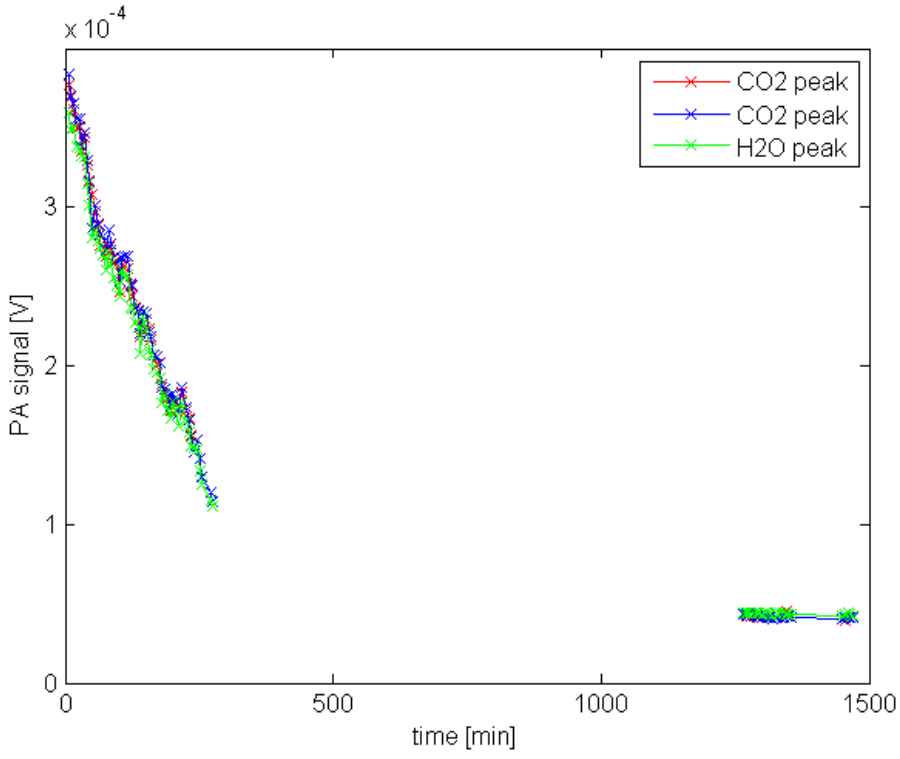

(b)

Figure 4.5: The PA signal from the water sample decrease with time until settling at a certain value. Figure 4.5a shows this in a 3D plot, while figure 4.5b shows the maximum value of the three peaks from figure 4.5a changing with time.

Chapter 5

Conclusion

The photoacoustic principle has been known of for more than 100 years, however it is only the 30 last years that a significant amount of research has been done on the subject. In this project, the goal was to determine if an affordable, low powered PA instrument for detecting CO_2 in gas and in water, could be developed.

In PA, a modulated laser light is absorbed by a sample and released as heat. The periodic adding of heat causes the illuminated part of the sample to expand and contract, generating pressure waves that can be measured using an acoustic transducer. The amplitude of the PA signal is linearly proportional to the absorption coefficient and to the concentration of the absorbing material. This linearity has been investigated and the measurements done on CO_2 in gas have given good results. The PA spectra shows three absorption peaks, and its maximum values has proven to be linear over several orders of magnitude. A theoretical detection limit of 20 *ppm* and an accuracy of approximately 2% has been determined. The effect of water vapour in the measurement cell was investigated, as well as the importance of having the right parameters.

PA measurements for CO_2 in water has been achieved, although not in a fully satisfying way. No signal was found directly using a hydrophone. A PA signal was however found using a microphone set to measure the PA effect in a layer of inert gas directly above the water surface. This technique allows for CO_2 to diffuse into the inert gas, ultimately making the PA signal a measurement of the amount of CO_2 that has diffused from the water, not

the amount in the water. An equilibrium state between the CO_2 in the water and the CO_2 in the gas takes hours to achieve. The change in amplitude of the signal over time indicates the rate of diffusion, so the amplitude can no longer be exclusively attributed to a change in concentration. This is not a fast, simple measuring instrument, in its current configuration.

To achieve these results, equipment for generating modulated laser light and for detecting the acoustic signal have been acquired and assembled. The measurement cell for gas detection was designed to exploit the effect of resonance, whereas the cell for water was designed first to hold a hydrophone, and later for holding a gas layer and a microphone. LabVIEW software was developed to automatise the spectroscopy measurements.

5.1 Further work

5.1.1 Ocean water

Quite a lot of research has already been done on CO_2 contents in the atmosphere. Less research has been done on CO_2 in water. That is why PAS performed in water would be interesting to investigate further. In the gas-phase results it was shown that mixing only CO_2 and N_2 did not necessarily give the same PA amplitude as natural air. The presence of other gases in the atmosphere may have enhanced the way CO_2 absorb or emit energy. The same may be true for liquid-phase samples. The presence of salt and biological material in the ocean water may give a different result than the clean water or the mineral water used in a laboratory, even if the CO_2 content is the same.

5.1.2 Experimenting with the configuration

In this project, different measurement cells was used for the gas-phase and water-phase measurements. In section 1.4 it was explained that the goal was to have an instrument that could measure CO_2 in both gas and water. It should be investigated if there exists a measurement cell configuration that works for both gas and water samples. Also, instead of using a microphone, the use of a PZT or PZTs should be investigated. Not only in the form of a hydrophone, but also in the form of more affordable PZTs. There's no limit to the possible variations available: Forward mounted, side mounted, flat, curved, even designing a measurement cell made entirely of piezoelectric material is possible.
Most importantly, a smaller measurement cell should be designed with the intention to decrease the noise level. The possibility of using the configuration with a hydrophone should be revisited due to the complications that arise with diffusivity between water and gas in the latest configuration. It is possible that the laser is simply not powerful enough to generate a PA signal in water, and the CO_2 must be measured via gas. In this case it is all the more important to decrease the volume of the measurement cell, and in this way decrease the time it takes to reach equilibrium.

5.1.3 Prototype

The equipment used in the lab takes up a lot of space and consists of several different instruments connected together. Each instrument can be used to many other things than what it is being used for. In order for this instrument to be tested in an industry environment, a prototype should be made. All the desired functions should be incorporated into one instrument, and all the unused functions should be removed. The instrument can then be calibrated and tested in an industrial environment.

References

Ainslie, M. A., and McColm J. G., 1998 "A simplified formula for viscous and chemical absorption in sea water". Journal of the Acoustical Society of America, 103(3), 1671-1672.

Ball, David W. 2006 "Photoacoustic Spectroscopy". Spectroscopy, Volume 21, Issue 9.

Bijnen, F.G.C., Reuss, J. and Harren F. J. M. 1996 "Geometrical optimization of a longitudinal resonant photoacoustic cell for sensitive and fast trace gas detection". Rev. Sci. Instrum. 67, 2914.

Cobbold, Richard S. C. 2007 "Foundations of Biomedical Ultrasound". New York: Oxford University Press.

De$\grave{a}$k, Rhea, Iwaki and Dlott 2000 "Vibrational Energy Relaxation and Spectral Diffusion in Water and Deuterated Water", J.Phys. Chem A, 104(21) pp 4866-4875.

Freeman, T. Picture of PA on melanoma. URL retrieved 27.05.2013: http://medicalphysicsweb.org/cws/article/research/48435

Gebhardt, F.G. and Smith, D.C. 1972 "Kinetic cooling of a gas by absorption of CO2 laser radiation". Applied Physics Letters 20(3), pp. 129–32.

Herbert and Bronwyn 2012 "High CO_2 in ocean can cause brain damage in fish". Australian Broadcasting Corporation. URL retrieved 27.05.2013: http://www.abc.net.au/am/content/2012/s3413187.htm

Kauppinen, J., Koskinen, V., Uotila, J. and Kauppinen, I. 2004 "Extremely sensitive CWA analyzer based on a novel optical pressure sensor in photoacoustic gas analysis". Proc. of SPIE 5617, pp. 115-127.

Keeling and Charels 2004 "Unsolved CO_2 mystery". Environment, vol 46 issue 10.

Krishnan, K. 1981 "Some Applications of Fourier Transform Infrared Photoacoustic Spectroscopy". Applied Spectroscopy, Vol. 35, Issue 6, pp. 549-557.

Michaelian, K. H. 2010 "Photoacoustic IR Spectroscopy". Wiley-VCH Verlag GmbH.

NDT Resource centre "Reflection and Transmission Coefficients". URL retrieved 28.05.2013: http://www.ndt-ed.org/EducationResources/CommunityCollege/Ultrasonics/Physics/reflectiontransmission.htm

Nguyen 2010 "VEP3001 lecture notes". Not published, included on CD.

NPL "Calculation of absorption of sound in seawater". ULR retrieved 27.05.2013: http://resource.npl.co.uk/acoustics/techguides/seaabsorption/

Patel, C. K. N. and Tam, A. C. 1981 "Pulsed optoacoustic spectroscopy of condensed matter". Rev. Mod. Phys, Vol. 53, No. 3.

Rosencwaig A. 1973 "Photoacoustic Spectroscopy of Biological Materials". New Series, American Association for the Advancement of Science, Vol. 181, No. 4100, pp. 657-658.

Rosencwaig, A. 1980 "Photoacoustics and Photoacoustic Spectroscopy". New York: John Wiley & Sons.

Schlageter et al. 1997 "Development of an optoacoustic sensor module for pH and/or CO_2 determination in aqueous solutions". Sensors and actuators B 38-39.

Schmid et al. 2009 "Optical Absorbance Measurements of Opaque Liquids by Pulsed Laser Photoacoustic Spectroscopy". Anal. Chem., 81, pp. 2403-2409.

Stanford Research Systems "About lock-in amplifiers", URL retrieved 25.05.2012: http://www.thinksrs.com/support/app.htm

Tyndall, J. 1881 "Action of an Intermitten Beam of Radiant Heat upon Gaseous Matter". Proc. Roy. Soc. London 31, 307.

Vestrheim, M. 2003 "Lecture notes for PHYS272". Department of Physics and Technology, University of Bergen. Not published.

Wieliczka, Weng and Querry 1989 "Wedge shaped cell for highly absorbent liquids: infrared optical constants of water". Applied optics 28, pp. 1714-1719.

Zhao and Zuomin 2002 "Pulsed photoacoustic techniques and glucose determination in human blood and tissue". Dept. of Electrical Engineering and infotech Oulu, University of Oulu.

Appendix A

This section describes the contents of the appended CD, and is shown in table 6.1.

Folder name	File(s) or folder name	Description
Datasheets	Agilent 33500B	Datasheet for the Agilent function generator used in this project.
	Bruel Kjaer Hyd.	Product data for the 8103, 8104, 8105 and 8106 hydrophones from Brüel & Kjær.
	Nanoplus DFB laser	Data sheet for the 2004 nm DFB laser from nanoplus.
	OpAmp AD797ANZ	Description of pre-amplifier used with the Sennheiser microphone, from Analog Devices.
	Sennheiser mic.	Technical data for the condenser microphone used in this project.
	SRS LIA	Manual for the LIA used in this project.
	Thorlabs ITC4005	Operational manual for the laser diode current and temperature controller used in this project.
Documents	PA cell	Information on the gas meas. cell.
Frequency sweep VI	freqsweep	Software used to determine resonance frequency in measurement cells.
	LIA	Support VIs for LIA communications.
PA Spectroscopy VI	Agilent support	Support VIs for agilent communications.
	funcgentalk	Sub VI for agilent communications.
	LIAinit	Sub VI for initialising LIA.
	LIAtalk	Sub VI for communications with LIA.
	Main	Main program for PA spectroscopy.
VEP3001	Photonics Week 02-11	Lecture notes by T. Nguyen.

Table 5.1: Listed content of appended CD.